[Short title + Author Name - P&H title] 17 (2024) 105528

Contents lists available at ScienceDirect

Arabian Journal of Chemistry

journal homepage: www.ksu.edu.sa

Treatment of rheumatoid arthritis with dissymmetric fluorine and pyridyl-substituted 3,5-bis(aryl)-4-piperidone derivatives by inhibition of NF-κB and MAPK activation

Wei-Bin Yan [a,b,1], Wen-Xuan Li [a,1], Yue Zhang [a], Lu Yu [a], Yu-Lun Li [a], Yong-Jun Liu [a,c], Gui-Ge Hou [a], Qing-Guo Meng [d,***], Li-Ying Ma [a,**], Zi-Kai Geng [a,*]

[a] School of Pharmacy, The Key Laboratory of Prescription Effect and Clinical Evaluation of State, Administration of Traditional Chinese Medicine of China, Binzhou Medical University, Yantai 264003, PR China
[b] Pharmacy Department, Sunshine Union Hospital, Weifang 261072, China
[c] Department of Chinese Medicine, Shandong Drug and Food Vocational College, Weihai, Shandong, China
[d] Department of Key Laboratory of Molecular Pharmacology and Drug Evaluation, School of Pharmacy, Yantai University, Yantai 264005, China

ARTICLE INFO

Keywords:
Rheumatoid arthritis (RA)
3,5-Bis(arylidene)-4-piperidone derivatives (BAPs)
Anti-inflammation
NF-κB
MAPK

ABSTRACT

Inhibition of inflammation-related NF-κB and MAPK activation could treat rheumatoid arthritis (RA). Previously, some fluorine-substituted 3,5-bis(aryl)-4-piperidone derivatives (BAPs) exhibited promising anti-inflammatory activity. Herein, interesting structural optimization was carried out and generated thirty-eight dissymmetric fluorine and pyridyl-substituted BAPs (**4a-s** and **5a-s**). They were confirmed by NMR and HRMS. A preliminary structure–activity relationship was summarized and discovered 3,5-CF_3 and 3-pyridyl-substituted **4k** exhibited less toxicity and higher anti-inflammatory activity. Preliminary mechanistic studies revealed that **4k** inhibited Lipopolysaccharide-induced nuclear factor kappa-B (NF-κB) and mitogen-activated protein kinase (MAPK) activation by suppressing LPS-induced phosphorylation levels of NF-κB/p65, NF-κB/IκBα, c-Jun N-terminal kinase (JNK), extracellular regulated protein kinases (ERK), and NF-κB/p38 in RAW264.7 cells. *In vivo*, **4k** inhibited the development of inflammation and synovial proliferation in rat joint tissues, significantly decreasing paw swelling and arthritis index in adjuvant-induced arthritis rats. More importantly, **4k** did not affect body weight and splenic index values. Overall, **4k** showed optimistic anti-RA effects, which may be developed as a potential multifunctional agent for the clinical treatment of RA.

1. Introduction

Rheumatoid arthritis (RA) is an autoimmune disease characterized by synovial cell hyperplasia, joint swelling, and joint pain (Bottini and Firestein, 2013; Nugroho and Morita, 2014; Wang et al., 2019). The clinical symptoms of RA are mainly inflammatory lesions in multiple joints throughout the body, characterized by chronic, peripheral, and symmetrical nature in its onset (Littlejohn and Monrad, 2018). As the disease progresses, RA affects multiple other organs in other parts of the body such as the heart, lungs, and kidneys. Both nuclear factor-κB (NF-κB) and mitogen-activated protein kinase (MAPK) signaling pathways are classical inflammatory pathways that promote the proliferation and differentiation of osteoclasts, cause bone erosion and bone destruction, with important roles in the progression of RA (Wei et al., 2022). In studies of synovial cells from RA patients, inhibition of NF-κB pathway activation inhibited the development of arthritis and pathological

Abbreviations: AIA, adjuvant-induced arthritis; BAPs, 3,5-bis(arylidene)-4-piperidones; BAP 4k BAP, representative compound 4k; CCK-8, Cell Counting Kit-8; CFA, complete Freund's adjuvant; ERK, extracellular regulated protein kinases; IκB, inhibitory subunit of nuclear factor-Kappa B; JNK, c-Jun N-terminal kinase; LPS, Lipopolysaccharide; MAPK, mitogen-activated protein kinase; MTX, methotrexate; NF-κB, nuclear factor kappa-B; RA, rheumatoid arthritis; PDTC, Pyrrolidine dithiocarbamate; TNF-α, tumor necrosis factor-α; IL-6, interleukin-6.

* Corresponding author.
** Corresponding author.
*** Corresponding author.
E-mail addresses: qinggmeng@163.com (Q.-G. Meng), maliyingbz@163.com (L.-Y. Ma), gengzikai@126.com (Z.-K. Geng).
[1] These authors contribute equally to this work.

https://doi.org/10.1016/j.arabjc.2023.105528
Received 18 July 2023; Accepted 4 December 2023
Available online 7 December 2023

damage to the joints. The MAPK pathway is divided into three components: Extracellular signal-regulated kinase (ERK), c-Jun N-terminal kinase (JNK), and p38 MAPK. JNK and p38 are activated mainly by stress stimuli or inflammatory cytokines. They can both influence the development of inflammation (Behl et al., 2021; Chen et al., 2023). Elevated expression of NF-κB in synovial tissue of RA patients is associated with overexpression of inflammatory mediators such as TNF-α and IL-6. It has been shown that p38 can regulate the production of cytokines such as TNF-α by macrophages, while JNK inhibitors can effectively reduce bone destruction in adjuvant arthritic rats. The pathogenesis of RA involves chronic inflammation, and various inflammatory stimuli (such as bacterial endotoxin lipopolysaccharide (LPS) and other foreign antigens). Inflammatory stimuli can induce macrophages to migrate to the contact site to produce TNF-α, IL-6 and promote inflammation, so studies using macrophage activation can reflect the inflammatory process in RA.

Curcumin (Fig. 1) is a natural component with anti-inflammatory and anti-cancer activities, including anti-RA (Pourhabibi-Zarandi et al., 2021), but its clinical application is limited by its structural instability, low bioavailability, and false positives. Therefore, the optimization of curcumin analogs has received extensive attention based on the pharmacodynamic structure of curcumin and literature reports. Among them, (3*E*,5*E*)-3,5-bis(arylidene)-4-piperidone (BAP) is a typical example, which has good anti-inflammatory and antitumor activities by inhibiting the activation of NF-κB. For example, fluorine-substituted 3,5-bis(2-fluorobenzylidene)-4-piperidone (EF**24**, Fig. 1) can inhibit tumor growth and metastasis by inhibiting NF-κB signaling pathways (He et al., 2018). An alkylated mono-carbonyl analog of curcumin (MAC **7a**, Fig. 1) showed potent anti-inflammatory activities against LPS-induced acute lung injury (ALI) in rats by inhibiting the expression of IL-6, IL-1*β*, TNF-α, and VCAM-1 in Beas-2B cells (Zhu et al., 2016). In recent years, our group obtained a number of BAPs and evaluated their anti-inflammatory activity, as well as toxicity. We found that some BAPs (e.g. BAP **6d**, BAP **32**, BAP **67**, Fig. 1) also showed good inhibition of MAPK signaling pathway, or were associated with NF-κB signaling pathway (Li et al., 2018a, 2018b; Yao et al., 2019). Structural analysis shows that these active compounds all contain different substituents, such as pyridyl, fluorophenyl, and trifluoromethylphenyl groups on both sides of 4-piperidone. On the one hand, the dissymmetric molecular structure may be more conducive to the interaction between lead compounds and targeted biological macromolecules. On the other hand, it is expected that the optimization of the different substituents will further optimize the water-solubility, toxicity, and bioactivity (Gao et al., 2020; Li et al., 2018a, 2018b). Therefore, the development of novel dissymmetric BAPs with different substituents for anti-inflammatory activity drug screening is of great research value.

Literature reports show that fluorine substitution can influence the potency, conformation, metabolism, membrane permeability, P-gp recognition of a molecule, and temper inhibition of the hERG channel by basic amines (Meanwell, 2018). Meanwhile, the electronegative fluorine substitution can form multiple H-bonds with the target protein (Swallow, 2015). In addition, pyridine substituent, as one of the imperative pharmacophores occurring synthetically as well as naturally in heterocyclic compounds, showed a wide range of therapeutic applications in the area of drug discovery, and many pyridine-based derivatives are reported to inhibit enzymes, receptors, and many other targets for controlling and curing the global serious diseases (Al-Warhi et al., 2023). Previously, our group reported that a group of fluorine or pyridyl-substituted BAPs derivatives could reasonably bind to the active site of Bcl-2, p65, and p38 proteins through multiple hydrogen bonds and halogen (fluorine) bonds (Sun et al., 2020; Sun et al., 2019; Cong et al., 2021). On this basis, our interests lie in the incorporation of different substituents (e.g. 3- or 4-pyridyl substituents, -F or -CF_3 substituents) on both sides of BAPs to report some dissymmetric BAPs. The

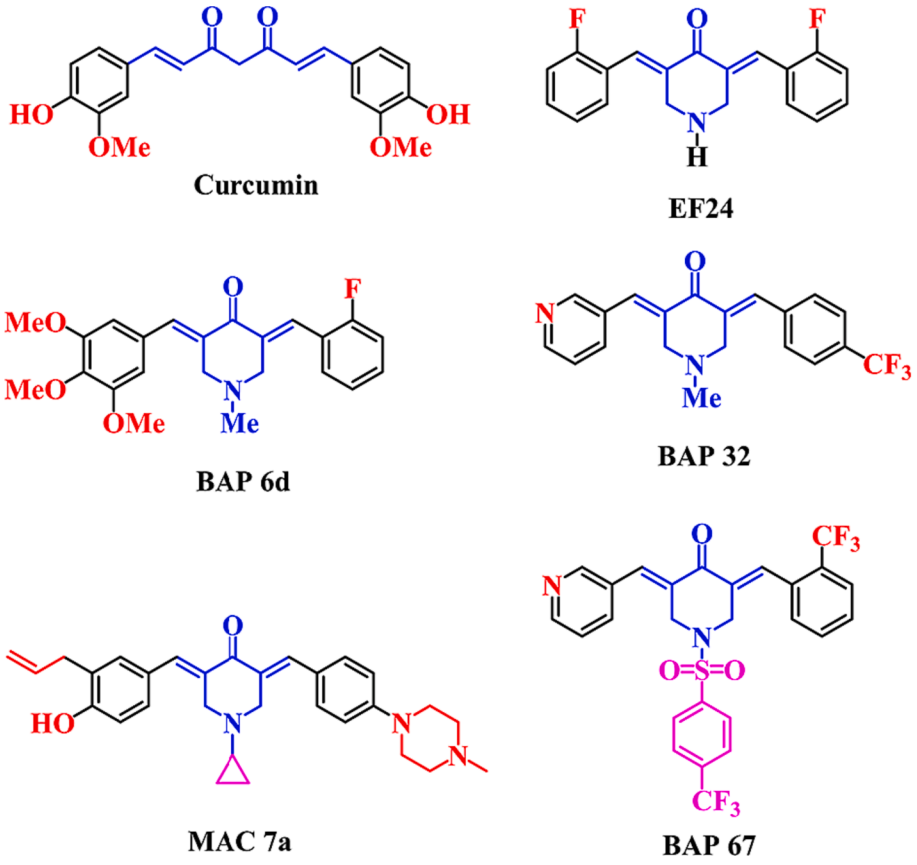

Fig. 1. The structures of curcumin and some BAPs were reported.

desired and improved anti-inflammatory activity of BAPs for the treatment of RA could be found. According to the above reasons, a series of dissymmetric fluorine and pyridyl-substituted BAPs were synthesized and evaluated as potential anti-inflammatory agents for the treatment of RA by inhibition of MAPK and NF-κB signaling pathways in this study. It is hoped that our study will yield potentially versatile drugs for the treatment of inflammatory diseases such as RA.

2. Experimental

2.1. Materials and methods

Chemical reagents such as fluorobenzene, pyridine benzene, all fragrant aldehydes, and piperidones had been then procured from Leyan Technology Co., Ltd (Beijing, China) and Bide Pharmaceutical Technology Co., Ltd. (Shanghai, China). Referring to the literature synthesis methods (Li et al., 2018a, 2018b), BAP derivatives (**4a-s**, **5a-s**) have been synthesized. Spectral records had been accumulated through the usage of ^{1}H NMR, Bruker Avance four hundred MHz or 600 MHz spectrometer and ^{13}C NMR, Bruker Avance one hundred MHz or a hundred and fifty MHz spectrometer in dimethyl sulfoxide (DMSO-d_6) solvent with tetramethylsilane (TMS) as inner standard. Chemical shifts (δ) are given in ppm and coupling constants (*J*) are given in Hz. All melting factors had been measured on a digital melting factor meter barring correction.

2.2. General procedure for the preparation of asymmetric BAP derivatives 4a-s

To 5 mL of methanol was once introduced 3-pyridinobenzaldehyde (0.54 g, 5.00 mmol), *N*-methylpiperidone (0.57 g, 5.00 mmol), and 3-fluorobenzaldehyde (0.62 g, 5.00 mmol). 2 mL of 10 % NaOH answer was brought at 25 °C and stirred for 6.0 h, all through which the response was observed via TLC. After the reaction, the precipitate was withdrawn and filtered, and the used to be subjected to silica gel column chromatography (petroleum ether: ethyl acetate: methanol = 10: 10: 1) to reap compound **4a** as a yellow solid. Compound **4b-s** was prepared in accordance with the instruction approach of compound **4a**.

2.2.1. (E)-3-((E)-3-fluorobenzylidene)-1-methyl-5-(pyridin-3-ylmethylene)piperidin-4-one (4a)

Yellow powder; yield: 67 %; Mp:136.3 ~ 137.6 °C; ^{1}H NMR (600 MHz, DMSO-d_6) δ 8.72 (d, J = 2.3 Hz, 1H), 8.59 (dd, J = 4.9, 1.6 Hz, 1H), 7.92 (dt, J = 8.0, 2.0 Hz, 1H), 7.60 (dd, J = 7.3 Hz, 2H), 7.52 (dt, J = 13.5, 7.8 Hz, 2H), 7.35 (t, J = 7.9 Hz, 2H), 7.30–7.24 (td, J = 8.6, 2.6 Hz, 1H), 3.75 (s, 2H), 3.75 (s, 2H), 2.40 (s, 3H). ^{13}C NMR (100 MHz, DMSO-d_6) δ 183.31, 162.09 (d, J = 243.3 Hz), 151.17, 149.66, 137.18, 136.89 (d, J = 8.5 Hz), 135.43, 134.69, 133.53 (d, J = 2.4 Hz), 131.37, 130.71 (d, J = 8.6 Hz), 130.53, 126.60, 123.73, 116.84 (d, J = 22.2 Hz), 116.09 (d, J = 22.2 Hz), 56.15, 46.58. HRMS (ESI): *m/z* calcd. for $C_{19}H_{17}FN_2O$, $[M + H]^+$, 309.1398; found: 309.1400.

2.2.2. (E)-3-((E)-4-fluorobenzylidene)-1-methyl-5-(pyridin-3-ylmethylene)piperidin-4-one (4b)

Yellow powder; yield: 68 %; Mp:135.2 ~ 136.8 °C; ^{1}H NMR (600 MHz, DMSO-d_6) δ 8.72 (s, 1H), 8.59 (d, J = 4.8 Hz, 1H), 7.92 (dt, J = 8.2, 2.2 Hz, 1H), 7.63–7.56 (m, 4H), 7.50 (dd, J = 7.9, 4.8 Hz, 1H), 7.32 (t, J = 8.8 Hz, 2H), 3.74 (s, 2H), 3.74 (s, 2H), 2.40 (s, 3H). ^{13}C NMR (150 MHz, DMSO-d_6) δ 186.70, 162.88(d, J = 247.5 Hz), 151.59, 150.06, 137.61, 135.98, 134.34, 133.74 (d, J = 2.5 Hz), 133.38 (d, J = 8.5 Hz), 131.60, 131.04, 124.18, 116.28 (d, J = 21.1 Hz), 56.74, 56.61, 45.72. HRMS (ESI): *m/z* calcd. for $C_{19}H_{17}FN_2O$, $[M + H]^+$, 309.1398; found: 309.1398.

2.2.3. (E)-1-methyl-3-(pyridin-3-ylmethylene)-5-((E)-3-(trifluoromethyl)benzylidene)piperidin-4-one (4c)

Yellow powder; yield: 55 %; Mp:129.7 ~ 131.5 °C; ^{1}H NMR (600 MHz, DMSO-d_6) δ 8.74 (d, J = 1.8 Hz, 1H), 8.60 (dd, J = 4.7, 1.2 Hz, 1H), 7.94 (d, J = 8.0 Hz, 1H), 7.67 (t, J = 7.3 Hz, 2H), 7.61–7.49 (m, 2H), 7.46 (s, 1H), 7.29–7.19 (m, 2H), 3.78 (s, 2H), 3.36 (s, 2H), 2.32 (s, 3H). ^{13}C NMR (150 MHz, DMSO-d_6) δ 186.75, 151.66, 150.15, 137.66, 136.09, 135.85, 135.61, 134.27, 133.73, 132.01, 129.99 (q, J = 31.5 Hz), 127.44 (q, J = 4.5 Hz), 126.05 (q, J = 4.0 Hz), 124.52(d, J = 271.5 Hz), 124.21, 56.53, 56.53, 45.60. HRMS (ESI): *m/z* calcd. for $C_{20}H_{17}F_4N_2O$, $[M + H]^+$, 377.1272; found: 377.1284.

2.2.4. (E)-3-((E)-2,3-difluorobenzylidene)-1-methyl-5-(pyridin-3-ylmethylene)piperidin-4-one (4d)

Yellow powder; yield: 70 %; Mp:134.6 ~ 136.2 °C; ^{1}H NMR (600 MHz, DMSO-d_6) δ 8.73 (d, J = 2.3 Hz, 1H), 8.60 (dd, J = 4.8, 1.6 Hz, 1H), 7.93 (dt, J = 7.9, 2.0 Hz, 1H), 7.64 (t, J = 2.2, 2H), 7.56–7.47 (m, 2H), 7.36–7.26 (m, 2H), 3.77 (s, 2H), 3.64 (s, 2H), 2.37 (s, 3H). ^{13}C NMR (150 MHz, DMSO-d_6) δ 186.34, 151.70, 150.31 (dd, J = 244.5, 12.0 Hz), 150.22, 148.48 (dd, J = 250.0, 12.8 Hz), 137.71, 136.89, 135.62, 132.57, 130.92, 126.58, 126.00, 125.52 (d, J = 9.9 Hz), 125.04 (d, J = 9.9 Hz), 124.20, 118.81 (d, J = 16.8 Hz), 56.72, 56.33, 45.56. HRMS (ESI): *m/z* calcd. for $C_{19}H_{17}F_2N_2O$, $[M + H]+$, 327.1304; found: 377.1305.

2.2.5. (E)-3-((E)-3,4-difluorobenzylidene)-1-methyl-5-(pyridin-3-ylmethylene)piperidin-4-one (4e)

Yellow powder; yield: 59 %; Mp:127.2 ~ 128.9 °C; ^{1}H NMR (600 MHz, DMSO-d_6) δ 8.71 (d, J = 2.3 Hz, 1H), 8.59 (dd, J = 4.8, 1.5 Hz, 1H), 7.91 (dt, J = 8.1, 2.2 Hz, 1H), 7.66–7.58 (m, 2H), 7.58–7.47 (m, 3H), 7.38 (m, 1H), 3.76 (s, 2H), 3.71(s, 2H), 2.40 (s, 3H). ^{13}C NMR (150 MHz, DMSO-d_6) δ 186.70, 151.64, 150.21(dd, J = 249.0 Hz, 12 Hz), 149.79 (dd, J = 244.5 Hz, 12 Hz), 137.64 (d, J = 9.9 Hz), 135.86, 134.91, 133.21, 132.71 (d, J = 9.9 Hz), 131.85, 128.28, 124.19, 119.82 (d, J = 17.4 Hz), 118.35 (d, J = 17.4 Hz), 56.60, 56.48, 45.67. HRMS (ESI): *m/z* calcd. for $C_{19}H_{17}F_2N_2O$, $[M + H]+$, 327.1304; found: 377.1303.

2.2.6. (E)-3-((E)-2,4-difluorobenzylidene)-1-methyl-5-(pyridin-3-ylmethylene)piperidin-4-one (4f)

Yellow powder; yield: 56 %; Mp:147.0 ~ 149.0 °C; ^{1}H NMR (600 MHz, DMSO-d_6) δ 8.62 (d, J = 2.3 Hz, 1H), 8.49 (dd, J = 4.8, 1.6 Hz, 1H), 7.82 (dt, J = 8.0, 2.0 Hz, 1H), 7.52 (d, J = 8.7 Hz, 2H), 7.44 (td, J = 8.8, 6.5 Hz, 1H),7.40 (dd, J = 7.8, 4.9 Hz, 1H),7.30 (ddd, J = 10.9, 9.3, 2.6 Hz, 1H), 7.11 (td, J = 9.8, 2.6 Hz,1H), 3.65 (s, 2H), 3.65 (s, 2H), 2.40 (s, 3H). ^{13}C NMR (150 MHz, DMSO-d_6) δ 186.36, 162.26 (dd, J = 249.0, 12.5 Hz), 161.22 (dd, J = 250.5, 12.4 Hz), 151.67, 150.18, 137.68, 135.70, 135.66, 132.76 (d, J = 9.9 Hz), 132.34, 130.97, 126.33, 124.20, 119.41 (d, J = 21.9, 3.5 Hz), 112.52 (d, J = 21.9, 3.5 Hz), 105.01 (t, J = 26.4 Hz), 56.72, 56.40, 45.60. HRMS (ESI): *m/z* calcd. for $C_{19}H_{17}F_2N_2O$, $[M + H]+$, 327.1304; found: 377.1304.

2.2.7. (E)-3-((E)-2,5-difluorobenzylidene)-1-methyl-5-(pyridin-3-ylmethylene)piperidin-4-one (4g)

Yellow powder; yield: 42 %; Mp:156.1 ~ 157.2 °C; ^{1}H NMR (600 MHz, DMSO-d_6) δ 8.73 (d, J = 2.1 Hz, 1H), 8.60 (dd, J = 4.8, 1.5 Hz, 1H), 7.93 (dt, J = 8.0, 2.0 Hz, 1H), 7.64 (s, 1H), 7.59 (s, 1H), 7.51 (dd, J = 7.9, 4.8 Hz, 1H), 7.43–7.31 (m, 3H), 3.77 (s, 2H), 3.66 (s, 2H), 2.38 (s, 3H). ^{13}C NMR (150 MHz, DMSO-d_6) δ 186.39, 158.32(d, J = 240 Hz), 157.02 (d, J = 244.02 Hz), 151.70, 150.22, 137.70, 136.87, 135.62, 132.52, 130.91, 126.19, 124.20, 124.10 (dd, J = 24.9, 8.6 Hz), 118.33 (dd, J = 24.2, 9.1 Hz), 117.80 (dd, J = 25.1, 9.2 Hz), 117.45 (d, J = 24.9 Hz), 56.72, 56.13, 45.55. HRMS (ESI): *m/z* calcd. for $C_{19}H_{17}F_2N_2O$, $[M + H]+$, 327.1304; found: 377.1308.

2.2.8. (E)-3-((E)-2,6-difluorobenzylidene)-1-methyl-5-(pyridin-3-ylmethylene)piperidin-4-one (4h)

Yellow powder; yield: 33 %; Mp:136.4 ~ 138.0 °C; ^{1}H NMR (600 MHz, DMSO-d_6) δ 8.74 (d, J = 1.8 Hz, 1H), 8.60 (dd, J = 4.7, 1.2 Hz, 1H), 7.94 (d, J = 8.0 Hz, 1H), 7.67 (s, 1H), 7.61–7.49 (m, 2H), 7.46 (s, 1H), 7.24 (t, J = 8.2 Hz, 2H), 3.78 (s, 2H), 3.34 (s, 2H), 2.32 (s, 3H). ^{13}C NMR (150 MHz, DMSO-d_6) δ 185.74, 160.08 (d, J = 247.5 Hz), 160.04 (d, J = 247.5 Hz), 155.07, 151.92, 151.73, 150.27, 137.91, 136.51, 135.34, 133.20, 132.34 (t, J = 9.9 Hz), 130.90, 124.84, 124.20, 122.39, 112.51 (dd, J = 21.1 Hz, 4.7 Hz), 112.15 (t, J = 26.4 Hz). 56.90, 56.32, 45.40. HRMS (ESI): *m/z* calcd. for $C_{19}H_{17}F_2N_2O$, [M + H]+, 327.1304; found: 377.1307.

2.2.9. (E)-3-((E)-3,5-difluorobenzylidene)-1-methyl-5-(pyridin-3-ylmethylene)piperidin-4-one (4i)

Yellow powder; yield: 72 %; Mp:145.5 ~ 147.1 °C; ^{1}H NMR (600 MHz, DMSO-d_6) δ 8.73 (d, J = 2.2 Hz, 1H), 8.60 (dd, J = 4.8, 1.6 Hz, 1H), 7.93 (d, J = 8.0 Hz, 1H), 7.62 (s, 1H), 7.56 (s, 1H), 7.51 (dd, J = 8.0, 4.7 Hz, 1H), 7.33 (tt, J = 9.4, 2.4 Hz, 1H), 7.26 (d, J = 6.4 Hz, 2H), 3.76 (s, 2H), 3.76 (s, 2H), 2.40 (s, 3H). ^{13}C NMR (150 MHz, DMSO-d_6) δ 186.76, 162.76 (d, J = 245.1, 13.6 Hz), 151.67, 150.17, 138.44 (t, J = 9.8 Hz), 137.66, 136.22, 135.79, 132.82, 132.06, 130.92, 124.19, 113.77 (d, J = 25.8 Hz), 105.06 (t, J = 25.8 Hz), 56.59, 56.35, 45.61. HRMS (ESI): *m/z* calcd. for $C_{19}H_{17}F_2N_2O$, [M + H]+, 327.1304; found: 377.1307.

2.2.10. (E)-3-((E)-2,4-bis(trifluoromethyl)benzylidene)-1-methyl-5-(pyridin-3-ylmethylene)piperidin-4-one (4j)

Yellow powder; yield: 45 %; Mp:158.2.5 ~ 159.7 °C; ^{1}H NMR (600 MHz, DMSO-d_6) δ 8.74 (d, J = 2.2 Hz, 1H), 8.60 (dd, J = 4.8 Hz, 1.6 Hz, 1H), 8.18–8.10 (m, 2H), 7.94 (dt, J = 8.1 Hz, 2.0 Hz, 1H), 7.80–7.73 (m, 2H), 7.67 (d, J = 2.2 Hz, 1H), 7.51 (dd, J = 8.1 Hz, 4.8 Hz, 1H), 3.77 (s, 2H), 3.54 (s, 2H), 2.32 (s, 3H). ^{13}C NMR (150 MHz, DMSO-d_6) δ 186.18, 151.76, 150.33, 137.77, 135.35, 133.24, 132.65, 130.87, 130.14 (d, J = 4.5 Hz), 129.75 (q, J = 33.0 Hz), 129.12 (q, J = 30.0 Hz), 123.76 (q, J = 270.0 Hz), 123.67 (q, J = 271.5 Hz), 129.86, 129.64, 129.12 (dd, J = 61.3, 30.3 Hz), 124.23, 123.65 (q, J = 6 Hz), 56.72, 55.58, 45.35. HRMS (ESI): *m/z* calcd. for $C_{21}H_{17}F_6N_2O$, [M + H]+, 427.1240; found: 427.1247.

2.2.11. (E)-3-((E)-3,5-bis(trifluoromethyl)benzylidene)-1-methyl-5-(pyridin-3-ylmethylene)piperidin-4-one (4k)

Yellow powder; yield: 36 %; Mp:133.0 ~ 134.7 °C; ^{1}H NMR (600 MHz, DMSO-d_6) δ 8.74 (d, J = 2.3 Hz, 1H), 8.60 (dd, J = 4.8, 1.6 Hz, 1H), 8.15 (d, J = 7.9 Hz, 3H), 7.94 (dt, J = 8.1, 2.1 Hz, 1H), 7.77 (d, J = 2.2 Hz, 1H), 7.65 (d, J = 2.2 Hz, 1H), 7.52 (dd, J = 8.0, 4.8 Hz, 1H), 3.79 (s, 2H), 3.77 (s, 2H), 2.39 (s, 3H). ^{13}C NMR (150 MHz, DMSO-d_6) δ 186.63, 170.78, 151.71, 150.22, 137.73 (d, J = 13.7 Hz), 137.11, 135.70, 132.28 (d, J = 30.0 Hz), 131.04 (q, J = 31.5 Hz), 130.93 (d, J = 3.7 Hz), 124.21, 123.65 (q, J = 271.5 Hz), 56.57, 55.91, 45.40. HRMS (ESI): *m/z* calcd. for $C_{21}H_{17}F_6N_2O$, [M + H]+, 427.1240; found: 427.1242.

2.2.12. (E)-3-((E)-2-fluoro-3-(trifluoromethyl)benzylidene)-1-methyl-5-(pyridin-3-ylmethylene)piperidin-4-one (4l)

Yellow powder; yield: 57 %; Mp:133.3 ~ 135.1 °C; ^{1}H NMR (600 MHz, DMSO-d_6) δ 8.73 (d, J = 2.3 Hz, 1H), 8.60 (dd, J = 4.8, 1.6 Hz, 1H), 7.99–7.89 (m, 1H), 7.82 (dt, J = 28.8, 7.4 Hz, 2H), 7.73–7.60 (s, 2H), 7.58–7.42 (m, 2H), 3.78 (s, 2H), 3.64 (s, 2H), 2.33 (s, 3H). ^{13}C NMR (150 MHz, DMSO-d_6) δ 186.27, 157.43 (d, J = 249.7 Hz), 151.70, 150.23, 137.72, 137.34, 136.01, 135.56, 132.70, 130.89, 128.38 (d, J = 3 Hz), 125.59 (d, J = 3.9 Hz), 124.46 (d, J = 12.5 Hz), 124.21, 123.00 (q, J = 272.3 Hz), 117.56(dd, J = 30, 12.3 Hz), 56.71, 56.12, 45.50. HRMS (ESI): *m/z* calcd. for $C_{20}H_{17}F_4N_2O$, [M + H]+, 377.1272; found: 377.1279.

2.2.13. (E)-3-((E)-2-fluoro-4-(trifluoromethyl)benzylidene)-1-methyl-5-(pyridin-3-ylmethylene)piperidin-4-one (4m)

Yellow powder; yield: 40 %; Mp:123.8 ~ 125.3 °C; ^{1}H NMR (600 MHz, DMSO-d_6) δ 8.73 (d, J = 2.5 Hz, 1H), 8.60 (dd, J = 4.8 Hz, 1.6 Hz, 1H), 7.93 (dt, J = 8.0 Hz, 2.1 Hz 1H), 7.82 (dd, J = 10.4 Hz, 1.6 Hz, 1H), 7.74–7.59 (m, 4H), 7.54–7.45 (m, 1H), 3.78 (s, 2H), 3.65 (s, 2H), 2.37 (s, 3H). ^{13}C NMR (150 MHz, DMSO-d_6) δ 186.32, 160.42 (d, J = 249.0 Hz), 151.74, 150.27, 137.73 (q, J = 3.3 Hz), 135.56, 132.68 (d, J = 24.9 Hz), 131.49 (q, J = 32.4, 8.6 Hz), 127.09 (d, J = 13.4 Hz), 123.66 (q, J = 271.5 Hz), 121.96, 113.79 (d, J = 24.9 Hz), 56.74, 56.20, 45.52. HRMS (ESI): *m/z* calcd. for $C_{20}H_{17}F_4N_2O$, [M + H]+, 377.1272; found: 377.1276.

2.2.14. (E)-3-((E)-2-fluoro-5-(trifluoromethyl)benzylidene)-1-methyl-5-(pyridin-3-ylmethylene)piperidin-4-one (4n)

Yellow powder; yield: 41 %; Mp:133.0 ~ 134.7 °C; ^{1}H NMR (600 MHz, DMSO-d_6) δ 8.74 (d, J = 2.3 Hz, 1H), 8.60 (dd, J = 4.7, 1.6 Hz, 1H), 7.93 (dt, J = 7.9, 2.0 Hz, 1H), 7.89 (m, 1H), 7.81 (dd, J = 6.7, 2.4 Hz, 1H), 7.67–7.63 (m, 2H), 7.59 (t, J = 9.3 Hz, 1H), 7.51 (m, 1H), 3.79 (s, 2H), 3.61 (s, 2H), 2.36 (s, 3H). ^{13}C NMR (150, DMSO-d_6) δ 186.26, 162.43 (d, J = 254.6 Hz), 151.73, 150.25, 137.57, 137.41, 135.55, 132.74, 130.91, 129.09 (q, J = 10.0, 4.1 Hz), 128.66 (q, J = 4.1 Hz), 126.18, 126.01 (d, J = 33.0 Hz), 124.22, 124.12, 123.93 (q, J = 270.0 Hz), 117.81 (dd, J = 24.2, 9.2 Hz), 117.66 (d, J = 23.6 Hz), 56.72, 55.95, 45.44. HRMS (ESI): *m/z* calcd. for $C_{20}H_{17}F_4N_2O$, [M + H]+, 377.1272; found: 377.1275.

2.2.15. (E)-3-((E)-2-fluoro-6-(trifluoromethyl)benzylidene)-1-methyl-5-(pyridin-3-ylmethylene)piperidin-4-one (4o)

Yellow powder; yield: 42 %; Mp:133.0 ~ 134.7 °C; ^{1}H NMR (600 MHz, DMSO-d_6) δ 8.74 (d, J = 2.3 Hz, 1H), 8.61 (dd, J = 4.8, 1.6 Hz, 1H), 7.93 (dt, J = 8.0, 2.0 Hz, 1H), 7.79–7.65 (m, 4H), 7.62–7.48 (m, 2H), 3.77 (s, 2H), 3.26 (s, 2H), 2.28 (s, 3H). ^{13}C NMR (150 MHz, DMSO-d_6) δ 185.65, 159.14 (d, J = 246.9 Hz), 151.72, 150.30, 138.71, 137.78, 135.24, 133.54, 131.88 (d, J = 9.5 Hz), 130.87, 129.44 (q, J = 33.0 Hz), 124.81, 124.19, 123.71 (q, J = 276.0 Hz), 122.92, 121.48 (dd, J = 23.4, 4.7 Hz), 121.09 (d, J = 23.4 Hz), 56.70, 55.73, 45.20. HRMS (ESI): *m/z* calcd. for $C_{20}H_{17}F_4N_2O$, [M + H]+, 377.1272; found: 377.1278.

2.2.16. (E)-3-((E)-3-fluoro-4-(trifluoromethyl)benzylidene)-1-methyl-5-(pyridin-3-ylmethylene)piperidin-4-one (4p)

Yellow powder; yield: 38 %; Mp:147.0 ~ 149.0 °C; ^{1}H NMR (600 MHz, DMSO-d_6) δ 8.73 (d, J = 2.3 Hz, 1H), 8.60 (dd, J = 4.8, 1.6 Hz, 1H), 7.93 (dt, J = 8.1, 2.0 Hz, 1H), 7.87 (t, J = 7.9 Hz, 1H), 7.67 (d, J = 11.9 Hz, 1H), 7.63 (q, J = 2.3 Hz, 2H), 7.54 (dt, 2H), 3.77 (s, 2H), 3.77 (s, 2H), 2.40 (s, 3H). ^{13}C NMR (150 MHz, DMSO-d_6) δ 186.72, 160.02, 158.34(d, J = 252.0 Hz), 151.71, 150.23, 142.05 (d, J = 8.5 Hz), 137.44, 135.70, 132.32, 130.91, 127.98 (d, J = 4.7 Hz), 127.16 (d, J = 3.7 Hz), 124.22, 123.91, 122.10 (q, J = 271.5 Hz), 118.85 (d, J = 21.1 Hz), 116.86 (dd, J = 32.2, 12.4 Hz), 56.61, 56.31, 45.56. HRMS (ESI): *m/z* calcd. for $C_{20}H_{17}F_4N_2O$, [M + H]+, 377.1272; found: 377.1275.

2.2.17. (E)-3-((E)-3-fluoro-5-(trifluoromethyl)benzylidene)-1-methyl-5-(pyridin-3-ylmethylene)piperidin-4-one (4q)

Yellow powder; yield: 35 %; Mp:120.4 ~ 122.1 °C; ^{1}H NMR (600 MHz, DMSO-d_6) δ 8.72 (d, J = 2.3 Hz, 1H), 8.59 (dd, J = 4.9 Hz, 1.6 Hz, 1H), 7.92 (dt, J = 8.1 Hz, 2.0 Hz, 1H), 7.80–7.70 (m, 2H), 7.70–7.59 (m, 3H), 7.50 (dd, J = 7.9 Hz, 4.8 Hz, 1H), 3.83 (s, 2H), 3.69 (s, 2H), 2.39 (s, 3H). ^{13}C NMR (150 MHz, DMSO-d_6) δ 186.09, 161.78(d, J = 246.0 Hz), 151.09, 149.59, 136.06 (d, J = 7.7 Hz), 135.13, 131.84, 131.61 (dd, J = 32.7, 8.9 Hz), 131.01, 125.73, 123.93 (d, J = 4.7 Hz), 123.60, 123.01 (q, J = 271.5 Hz), 122.11, 120.47 (d, J = 21 Hz), 113.11 (dd, J = 24.8, 3.8 Hz), 55.98, 55.55, 44.92. HRMS (ESI): *m/z* calcd. for $C_{20}H_{17}F_4N_2O$, [M + H]+, 377.1272; found: 377.1277.

2.2.18. (E)-3-((E)-4-fluoro-2-(trifluoromethyl)benzylidene)-1-methyl-5-(pyridin-3-ylmethylene)piperidin-4-one (4r)

Yellow powder; yield: 39 %; Mp:164.0 ~ 166.0 °C; ^{1}H NMR (600 MHz, DMSO-d_6) δ 8.73 (d, J = 2.3 Hz, 1H), 8.60 (dd, J = 4.8, 1.6 Hz, 1H), 7.93 (dt, J = 8.1, 2.0 Hz, 1H), 7.87 (t, J = 7.9 Hz, 1H), 7.67 (d, J = 11.9 Hz, 1H), 7.63 (q, J = 2.3 Hz, 2H), 7.54 (dt, 2H), 3.77 (s, 2H), 3.76 (s, 2H), 2.40 (s, 3H). ^{13}C NMR (150 MHz, DMSO-d_6) δ 186.75, 159.19 (d, J = 253.6 Hz), 151.71, 150.23, 142.06 (d, J = 8.7 Hz), 137.71, 137.21, 135.74, 132.30, 130.92, 128.01 (q, J = 4.9 Hz), 127.15, 124.22, 123.01 (d, J = 271.9 Hz), 122.11, 118.85 (d, J = 21.1 Hz), 116.85 (d, J = 31.5 Hz),116.85 (d, J = 21.1 Hz), 56.63, 56.32, 45.57. HRMS (ESI): m/z calcd. for $C_{20}H_{17}F_4N_2O$, [M + H]+, 377.1272; found: 377.1274.

2.2.19. (E)-3-((E)-4-fluoro-3-(trifluoromethyl)benzylidene)-1-methyl-5-(pyridin-3-ylmethylene)piperidin-4-one (4s)

Yellow powder; yield: 43 %; Mp:126.5 ~ 128.5 °C; ^{1}H NMR (600 MHz, DMSO-d_6) δ 8.73 (d, J = 2.3 Hz, 1H), 8.60 (dd, J = 4.8, 1.6 Hz, 1H), 7.93 (ddt, J = 8.1, 4.0, 2.0 Hz, 2H), 7.90–7.84 (m, 1H), 7.68 (d, J = 2.1 Hz, 1H), 7.66–7.59 (m, 2H), 7.51 (ddd, J = 8.0, 4.8, 0.8 Hz, 1H), 3.77 (s, 2H), 3.76 (s, 2H), 2.39 (s, 3H). ^{13}C NMR (150 MHz, DMSO-d_6) δ 186.66, 159.26(d, J = 255.0 Hz), 151.66, 150.16, 137.66, 137.15 (d, J = 8.6 Hz), 135.83, 135.37, 132.82, 132.25, 132.01, 130.97, 129.96 (q, J = 4.7 Hz), 124.21, 122.88(q, J = 270.0 Hz), 118.17 (d, J = 20.8 Hz), 117.48 (qd, J = 33.0, 12.0 Hz), 56.60, 56.32, 45.59. HRMS (ESI): m/z calcd. for $C_{20}H_{17}F_4N_2O$, [M + H]+, 377.1272; found: 377.1275.

2.3. General procedure for the preparation of asymmetric BAP derivatives 5a-s

In a 25 mL beaker, dissolve 4-pyridinobenzaldehyde (0.54 g, 5.00 mmol), *N*-methylpiperidone (0.57 g, 5.00 mmol), and 3-fluorobenzaldehyde (0.62 g, 5.00 mmol) in 10 mL acetic acid Dry hydrogen chloride gas was consistently injected for forty-five min, and stirred at 25 °C for 10 h, at some point of which TLC tracked the reaction. After the reaction, the precipitate was withdrawn and filtered. After the precipitation is dissolved in distilled water, alter the pH value to 8–9 with 10 % NaOH solution. The resultant precipitation is subjected to silica gel column chromatography (Petroleum ether: Ethyl acetate: methanol = 10: 10: 1) to attain compound **5a** as a yellow solid. Compound **5b-s** was prepared in accordance with the instruction approach of compound **5a**.

2.3.1. (E)-3-((E)-3-fluorobenzylidene)-1-methyl-5-(pyridin-4-ylmethylene)piperidin-4-one (5a)

Yellow powder; yield: 65 %; Mp:107.5 ~ 109.1 °C; ^{1}H NMR (600 MHz, DMSO-d_6) δ 8.71–8.64 (m, 2H), 7.60 (s, 1H), 7.56–7.49 (m, 2H), 7.49–7.44 (m, 2H), 7.37 (t, J = 8.1 Hz, 2H), 7.29 (td, J = 8.7, 2.6 Hz, 1H), 3.76 (t, J = 2.6 Hz, 4H), 2.40 (s, 3H). ^{13}C NMR (150 MHz, DMSO-d_6) δ 186.92, 162.55 (d, J = 241.7 Hz), 150.51, 142.19, 137.71, 137.26 (d, J = 8.4 Hz), 135.05, 134.28, 132.24, 131.19 (d, J = 7.8 Hz), 127.11 (d, J = 3.2 Hz), 124.66, 117.35 (d, J = 22.3 Hz), 116.64 (d, J = 21.2 Hz), 56.60, 56.48, 45.63. HRMS (ESI): m/z calcd. for $C_{19}H_{17}FN_2O$, $[M + H]^+$, 309.1398; found: 309.1398.

2.3.2. (E)-3-((E)-4-fluorobenzylidene)-1-methyl-5-(pyridin-4-ylmethylene)piperidin-4-one (5b)

Yellow powder; yield: 63 %; Mp:145.4 ~ 147.4 °C; ^{1}H NMR (600 MHz, DMSO-d_6) δ 8.66 (d, J = 5.3 Hz, 2H), 7.66–7.55 (m, 3H), 7.52 (s, 1H), 7.45 (d, J = 4.9 Hz, 2H), 7.32 (t, J = 8.7 Hz, 2H), 3.74 (s, 2H), 3.74 (s, 2H), 2.39 (s, 3H). ^{13}C NMR (150 MHz, DMSO-d_6) δ 186.85, 162.94 (d, J = 246.5 Hz), 150.51, 142.27, 137.79, 134.66, 133.64, 133.46 (d, J = 8.1 Hz), 132.03, 131.54 (d, J = 3.5 Hz), 124.66, 116.32 (d, J = 21.2 Hz), 56.73, 56.49, 45.68. HRMS (ESI): m/z calcd. for $C_{19}H_{17}FN_2O$, $[M + H]^+$, 309.1398; found: 309.1403.

2.3.3. (E)-1-methyl-3-(pyridin-4-ylmethylene)-5-((E)-3(trifluoromethyl) benzylidene)piperidin-4-one (5c)

Yellow powder; yield: 52 %; Mp:104.7 ~ 106.4 °C; ^{1}H NMR (600 MHz, DMSO-d_6) δ 8.67 (dd, J = 4.6, 1.4 Hz, 2H), 7.86 (s, 1H), 7.79 (t, J = 7.3 Hz, 2H), 7.76–7.67 (m, 2H), 7.54 (s, 1H), 7.49–7.44 (m, 2H), 3.77 (dd, J = 4.1, 1.4 Hz, 4H), 2.39 (s, 3H). ^{13}C NMR (150 MHz, DMSO-d_6) δ 186.85, 150.52, 142.17, 137.65, 136.00, 135.74, 134.15, 134.01, 132.39, 130.31, 129.99 (q, J = 31.5 Hz), 127.74 (d, J = 3 Hz), 127.15, 126.11 (d, J = 3.4 Hz), 124.45(q, J = 271 Hz), 124.26, 56.45, 45.56. HRMS (ESI): m/z calcd. for $C_{20}H_{17}F_4N_2O$, [M + H]+, 377.1272; found: 377.1271.

2.3.4. (E)-3-((E)-2,3-difluorobenzylidene)-1-methyl-5-(pyridin-4-ylmethylene)piperidin-4-one (5d)

Yellow powder; yield: 65 %; Mp:136.2 ~ 138.1 °C; ^{1}H NMR (600 MHz, DMSO-d_6) δ 8.67 (dd, J = 4.5, 1.5 Hz, 2H), 7.65 (d, J = 8.5 Hz, 1H), 7.58–7.50 (s, 2H), 7.47 (dd, J = 4.8, 1.3 Hz, 2H), 7.32 (ddd, J = 9.1, 7.7, 4.9 Hz, 2H), 3.76 (s, 2H), 3.67 (s, 2H), 2.37 (s, 3H). ^{13}C NMR (150 MHz, DMSO-d_6) δ 186.47, 150.52, 150.36 (dd, J = 244.5, 12.8 Hz), 148.50 (dd, J = 247.5, 13.5 Hz), 142.09, 137.40, 136.75, 132.95, 126.56, 126.27, 125.52 (d, J = 9.9 Hz), 124.96 (d, J = 9.9 Hz), 124.67, 118.89 (d, J = 16.9 Hz), 56.57, 56.31, 45.51. HRMS (ESI): m/z calcd. for $C_{19}H_{17}F_2N_2O$, [M + H]+, 327.1304; found: 377.1307.

2.3.5. (E)-3-((E)-3,4-difluorobenzylidene)-1-methyl-5-(pyridin-4-ylmethylene)piperidin-4-one (5e)

Yellow powder; yield: 38 %; Mp:106.4 ~ 107.6 °C; ^{1}H NMR (600 MHz, DMSO-d_6) δ 8.75–8.61 (m, 2H), 7.68–7.60 (m, 1H), 7.59–7.49 (m, 3H), 7.45 (d, J = 5.1 Hz, 2H), 7.42–7.35 (m, 1H), 3.74 (s, 2H), 3.74 (s, 2H), 2.39 (s, 3H). ^{13}C NMR (150 MHz, DMSO-d_6) δ 186.38, 149.79 (dd, J = 247.5, 12.6 Hz), 149.33(dd, J = 244 0.5, 12.6 Hz), 137.20, 134.32, 133.04, 132.18 (d, J = 4.7 Hz), 127.89 (dd, J = 6.9, 3.1 Hz), 124.20, 119.40 (d, J = 17.4 Hz), 117.91 (d, J = 17.4 Hz), 55.99, 45.15. HRMS (ESI): m/z calcd. for $C_{19}H_{17}F_2N_2O$, [M + H]+, 327.1304; found: 377.1310.

2.3.6. (E)-3-((E)-2,4-difluorobenzylidene)-1-methyl-5-(pyridin-4-ylmethylene)piperidin-4-one (5f)

Yellow powder; yield: 52 %; Mp:164.0 ~ 166.0 °C; ^{1}H NMR (600 MHz, DMSO-d_6) δ 8.69–8.65 (m, 2H), 7.62 (s, 1H), 7.55 (s, 2H), 7.46 (d, J = 4.6 Hz, 2H), 7.45–7.35 (m, 1H), 7.22 (td, J = 8.4, 2.4 Hz, 1H), 3.76 (s, 2H), 3.64 (s, 2H), 2.37 (s, 3H). ^{13}C NMR (150 MHz, DMSO-d_6) δ 186.54, 163.34 (d, J = 249.0, 12.5 Hz), 161.25 (d, J = 250.5, 12.4 Hz), 150.54, 142.16, 137.50, 135.55, 132.77, 132.73, 126.62 (d, J = 9.9 Hz), 124.68, 119.35 (dd, J = 21.4, 3.6 Hz), 112.55 (dd, J = 21.1, 3.7 Hz), 105.04 (t, J = 26.4 Hz), 56.57, 56.38, 45.56. HRMS (ESI): m/z calcd. for $C_{19}H_{17}F_2N_2O$, [M + H]+, 327.1304; found: 377.1303.

2.3.7. (E)-3-((E)-2,5-difluorobenzylidene)-1-methyl-5-(pyridin-4-ylmethylene)piperidin-4-one (5g)

Yellow powder; yield: 53 %; Mp:161.0 ~ 163.0 °C; ^{1}H NMR (600 MHz, DMSO-d_6) δ 8.67 (d, J = 6.1 Hz, 2H), 7.59 (s, 1H), 7.55 (s, 1H), 7.47 (d, J = 6.3 Hz, 2H), 7.44–7.31 (m,3H), 3.76 (s,2H), 3.66 (s, 2H), 2.37 (s, 3H). ^{13}C NMR (150 MHz, DMSO-d_6) δ 186.57, 158.71 (dd, J = 240, 3 Hz), 157.05(dd, J = 244.5, 3 Hz), 150.55, 142.10, 137.43, 136.77, 132.92, 126.47, 124.69, 124.06 (dd, J = 24.9, 8.7 Hz), 118.44 (dd, J = 24.3, 9.1 Hz), 117.83 (dd, J = 24.9, 8.8 Hz), 117.46 (d, J = 25.0 Hz), 56.58, 56.12, 45.51. HRMS (ESI): m/z calcd. for $C_{19}H_{17}F_2N_2O$, [M + H]+, 327.1304; found: 377.1305.

2.3.8. (E)-3-((E)-2,6-difluorobenzylidene)-1-methyl-5-(pyridin-4-ylmethylene)piperidin-4-one (5h)

Yellow powder; yield: 30 %; Mp:133.0 ~ 134.7 °C; ^{1}H NMR (600 MHz, DMSO-d_6) δ 8.68 (d, J = 6.0 Hz, 2H), 7.61–7.52 (m, 2H), 7.49–7.43 (m, 3H), 7.24 (t, J = 8.2 Hz, 2H), 3.77 (s, 2H), 3.40 (s, 2H), 2.31 (s, 3H). ^{13}C NMR (150 MHz, DMSO-d_6) δ 185.97, 160.08 (d, J =

247.5 Hz), 160.03 (d, J = 247.5 Hz), 150.52, 142.09, 138.07, 137.23, 133.49, 132.43 (t, J = 10.5 Hz), 124.69, 122.63, 112.43 (dd, J = 21.2, 4.0 Hz), 112.09 (t, J = 19.7 Hz), 56.79, 56.32, 45.39. HRMS (ESI): *m/z* calcd. for $C_{19}H_{17}F_2N_2O$, [M + H]+, 327.1304; found: 377.1308.

2.3.9. (E)-3-((E)-3,5-difluorobenzylidene)-1-methyl-5-(pyridin-4-ylmethylene)piperidin-4-one (5i)

Yellow powder; yield: 66 %; Mp:139.0 ~ 140.9 °C; ^{1}H NMR (600 MHz, DMSO-d_6) δ 8.69–8.65 (m, 2H), 7.56 (d, J = 2.2 Hz, 1H), 7.53 (d, J = 2.2 Hz, 1H), 7.48–7.44 (m, 2H), 7.34 (tt, J = 9.3, 2.4 Hz, 1H), 7.27 (h, J = 4.7 Hz, 2H), 3.75 (dd, J = 4.4, 2.2 Hz, 4H), 2.39 (s, 3H). ^{13}C NMR (150 MHz, DMSO-d_6) δ 186.95, 162.79 (d, J = 245.3, 12.7 Hz), 150.54, 142.12, 138.37 (t, J = 9.8 Hz), 137.62, 136.13, 133.12, 132.46, 124.68, 113.83 (dd, J = 19.9, 5.1 Hz), 105.15 (t, J = 25.8 Hz), 56.46, 56.34, 45.57. HRMS (ESI): *m/z* calcd. for $C_{19}H_{17}F_2N_2O$, [M + H]+, 327.1304; found: 377.1306.

2.3.10. (E)-3-((E)-2,4-bis(trifluoromethyl)benzylidene)-1-methyl-5-(pyridin-4-ylmethylene)piperidin-4-one (5j)

Yellow powder; yield: 36 %; Mp:150.8 ~ 152.2 °C; ^{1}H NMR (600 MHz, DMSO-d_6) δ 8.71–8.61 (m, 2H), 8.23–8.02 (m, 2H), 7.83–7.68 (m, 2H), 7.58 (d, J = 2.2 Hz, 1H), 7.50–7.38 (m, 2H), 3.76 (s, 2H), 3.54 (s, 2H), 2.30 (s, 3H). ^{13}C NMR (150 MHz, DMSO-d_6) δ 186.33, 150.56, 142.03, 137.73 (d, J = 28.4 Hz), 137.13, 133.61, 132.64, 130.15 (d, J = 4.5 Hz), 129.92 (d, J = 34.5 Hz), 128.99 (d, J = 34.5 Hz), 123.75(q, J = 271.5 Hz), 123.66 (q, J = 273.0 Hz), 124.72, 123.67 (q, J = 4.5 Hz), 56.56, 55.55, 45.30. HRMS (ESI): *m/z* calcd. for $C_{21}H_{17}F_6N_2O$, [M + H]+, 427.1240; found: 427.1244.

2.3.11. (E)-3-((E)-3,5-bis(trifluoromethyl)benzylidene)-1-methyl-5-(pyridin-4-ylmethylene)piperidin-4-one (5k)

Yellow powder; yield: 38 %; Mp:131.5 ~ 132.5 °C; ^{1}H NMR (600 MHz, DMSO-d_6) δ 8.68 (dd, J = 4.5, 1.6 Hz, 2H), 8.16 (s, 3H), 7.77 (s, 1H), 7.56 (s, 1H), 7.47 (dd, J = 4.8, 1.3 Hz, 2H), 3.78 (s, 2H), 3.78 (s, 2H), 2.38 (s, 3H). ^{13}C NMR (150 MHz, DMSO-d_6) δ 186.79, 150.55, 142.06, 137.66, 137.49, 136.96, 137.57 (d, J = 25.1 Hz), 137.22, 132.64, 131.25 (d, J = 32.7 Hz), 131.03(q, J = 33 Hz), 130.98 (d, J = 3.7 Hz), 130.92, 124.68, 123.64 (q, J = 271 Hz), 122.80, 56.14, 45.37. HRMS (ESI): *m/z* calcd. for $C_{21}H_{17}F_6N_2O$, [M + H]+, 427.1240; found: 427.1243.

2.3.12. (E)-3-((E)-2-fluoro-3-(trifluoromethyl)benzylidene)-1-methyl-5-(pyridin-4-ylmethylene)piperidin-4-one (5l)

Yellow powder; yield: 55 %; Mp:133.6 ~ 134.6 °C; ^{1}H NMR (600 MHz, DMSO-d_6) δ 8.68 (d, J = 5.9 Hz, 2H), 7.83 (dt, J = 29.4, 7.2 Hz, 2H), 7.66 (s, 1H), 7.57 (s, 1H)7.54 (dd, J = 21.2, 13.4 Hz, 1H), 7.47 (d, J = 5.8 Hz, 2H), 3.78 (s, 2H), 3.66 (s, 2H), 2.36 (s, 3H). ^{13}C NMR (150 MHz, DMSO-d_6) δ 186.41, 157.46 (d, J = 257.8 Hz), 150.53, 142.06, 136.00, 133.07, 128.45, 125.87 (d, J = 4.8 Hz), 125.59 (d, J = 3.9 Hz), 123.49 (q, J = 270 Hz), 124.68, 124.39 (d, J = 12.4 Hz), 117.57 (dd, J = 32.3, 12.4 Hz), 56.56, 56.11, 45.46. HRMS (ESI): *m/z* calcd. for $C_{20}H_{17}F_4N_2O$, [M + H]+, 377.1272; found: 377.1270.

2.3.13. (E)-3-((E)-2-fluoro-4-(trifluoromethyl)benzylidene)-1-methyl-5-(pyridin-4-ylmethylene)piperidin-4-one (5m)

Yellow powder; yield: 32 %; Mp:129.7 ~ 131.1 °C; ^{1}H NMR (600 MHz, DMSO-d_6) δ 8.69–8.65 (m, 2H), 7.82 (dd, J = 10.4 Hz, 1.7 Hz, 1H), 7.69 (td, J = 8.7 Hz, 8.3 Hz, 4.2 Hz, 2H), 7.65 (m, 1H), 7.56 (d, J = 2.3 Hz, 1H), 7.49–7.45 (m, 2H), 3.77 (s, 2H), 3.65 (s, 2H), 2.36 (s, 3H). ^{13}C NMR (150 MHz, DMSO-d_6) δ 186.49, 160.44(d, J = 249.0 Hz), 150.55, 142.07, 137.61, 137.37, 133.13, 132.60 (d, J = 26.0 Hz), 131.55 (q, J = 32.5, 8.6 Hz), 127.01 (d, J = 13.4 Hz), 123.64 (q, J = 271.5 Hz), 126.12 (d, J = 3.8 Hz), 124.70, 124.55, 122.74, 121.97, 120.93, 113.80 (dd, J = 26.0, 3.9 Hz), 56.59, 56.17, 45.47. HRMS (ESI): *m/z* calcd. for $C_{20}H_{17}F_4N_2O$, [M + H]+, 377.1272; found: 377.1274.

2.3.14. (E)-3-((E)-2-fluoro-5-(trifluoromethyl)benzylidene)-1-methyl-5-(pyridin-4-ylmethylene)piperidin-4-one (5n)

Yellow powder; yield: 38 %; Mp:133.0 ~ 134.7 °C; ^{1}H NMR (600 MHz, DMSO-d_6) δ 8.68–8.67 (m, 2H), 7.90 (ddd, J = 8.6, 4.5, 2.3 Hz, 1H), 7.82 (dd, J = 6.7, 2.4 Hz, 1H), 7.64 (s, 1H), 7.61–7.56 (m, 2H), 7.48–7.46 (m, 2H), 3.78 (s, 2H), 3.62 (s, 2H), 2.35 (s, 3H). ^{13}C NMR (150 MHz, DMSO-d_6) δ 186.44, 162.45 (d, J = 254.5 Hz), 150.56, 142.08, 137.35 (d, J = 10.3 Hz), 133.12, 126.48 (dd, J = 9.8, 4.5 Hz), 126.39–125.64 (m), 124.70 (d, J = 31.1 Hz), 123.85 (d, J = 23.5 Hz), 123.75 (q, J = 270.0 Hz), 117.69 (d, J = 23.5 Hz), 56.56, 55.92, 45.39. HRMS (ESI): *m/z* calcd. for $C_{20}H_{17}F_4N_2O$, [M + H]+, 377.1272; found: 377.1277.

2.3.15. (E)-3-((E)-2-fluoro-6-(trifluoromethyl)benzylidene)-1-methyl-5-(pyridin-4-ylmethylene)piperidin-4-one (5o)

Yellow powder; yield: 41 %; Mp:133.0 ~ 134.7 °C; ^{1}H NMR (600 MHz, DMSO-d_6) δ 8.70–8.66 (m, 2H), 7.75–7.69 (m, 3H), 7.61 (d, J = 2.3 Hz, 1H), 7.53 (q, J = 2.3 Hz, 1H), 7.49–7.45 (m, 2H), 3.76 (d, J = 2.3 Hz, 2H), 3.27 (s, 2H), 2.27 (s, 3H). ^{13}C NMR (150 MHz, DMSO-d_6) δ 185.81, 159.14 (d, J = 247.0 Hz), 150.53, 142.06, 138.61, 137.00, 133.92, 131.93 (d, J = 9.5 Hz), 129.86 (d, J = 30.3 Hz), 125.16, 124.70, 123.71 (q, J = 273.0 Hz), 122.90, 121.39 (d, J = 19.7 Hz), 121.10 (d, J = 23.4 Hz), 56.54, 55.68, 45.14. HRMS (ESI): *m/z* calcd. for $C_{20}H_{17}F_4N_2O$, [M + H]+, 377.1272; found: 377.1276.

2.3.16. (E)-3-((E)-3-fluoro-4-(trifluoromethyl)benzylidene)-1-methyl-5-(pyridin-4-ylmethylene)piperidin-4-one (5p)

Yellow powder; yield: 38 %; Mp:164.0 ~ 166.0 °C; ^{1}H NMR (600 MHz, DMSO-d_6) δ 8.67 (d, J = 6.0 Hz, 2H), 7.87 (t, J = 8.0 Hz, 1H), 7.68 (d, J = 11.9 Hz, 1H), 7.63 (s, 1H), 7.54 (d, J = 10.4 Hz, 2H), 7.47 (d, J = 6.2 Hz, 2H), 3.77 (s, 2H), 2.39 (s, 3H). ^{13}C NMR (150 MHz, DMSO-d_6) δ 186.89, 160.05, 158.26 (d, J = 268.5 Hz), 150.55, 142.08, 141.95 (d, J = 8.8 Hz), 137.30, 132.65, 128.05 (d, J = 4.9 Hz), 127.20 (d, J = 3.7 Hz), 124.69, 122.24 (dq, J = 271.5 Hz), 118.89 (d, J = 21.1 Hz), 117.07 (dd, J = 33.1, 11.5 Hz), 56.47, 56.29, 45.52. HRMS (ESI): *m/z* calcd. for $C_{20}H_{17}F_4N_2O$, [M + H]+, 377.1272; found: 377.1279.

2.3.17. (E)-3-((E)-3-fluoro-5-(trifluoromethyl)benzylidene)-1-methyl-5-(pyridin-4-ylmethylene)piperidin-4-one (5q)

Yellow powder; yield: 35 %; Mp:162.8 ~ 164.2 °C; ^{1}H NMR (600 MHz, DMSO-d_6) δ 8.72–8.63 (m, 2H), 7.80–7.71 (m, 2H), 7.72–7.64 (m, 2H), 7.54 (d, J = 2.2 Hz, 1H), 7.50–7.42 (m, 2H), 3.77 (s, 2H), 3.77 (s, 2H), 2.39 (s, 3H). ^{13}C NMR (150 MHz, DMSO-d_6) δ 186.91, 162.40 (d, J = 246.0 Hz), 150.55, 142.10, 138.67 (d, J = 9.0 Hz), 137.59, 136.59, 132.68, 131.85 (dd, J = 32.3, 8.7 Hz), 124.53, 124.38, 123.81, 123.80 (d, J = 4.2 Hz), 123.60 (q, J = 271.5 Hz),122.73, 121.12 (d, J = 22.3 Hz), 113.73 (d, J = 25.6 Hz), 56.45, 56.14, 45.49. HRMS (ESI): *m/z* calcd. for $C_{20}H_{17}F_4N_2O$, [M + H]+, 377.1272; found: 377.1280.

2.3.18. (E)-3-((E)-4-fluoro-2-(trifluoromethyl)benzylidene)-1-methyl-5-(pyridin-4-ylmethylene)piperidin-4-one (5r)

Yellow powder; yield: 33 %; Mp:133.0 ~ 134.7 °C; ^{1}H NMR (600 MHz, DMSO-d_6) δ 8.69–8.65 (m, 2H), 7.78 (dd, J = 9.1, 2.7 Hz, 1H), 7.75 (d, J = 4.5 Hz, 1H), 7.65 (td, J = 8.5, 2.7 Hz, 1H), 7.61–7.54 (m, 2H), 7.49–7.45 (m, 2H), 3.76 (d, J = 2.4 Hz, 2H), 3.54 (d, J = 2.0 Hz, 2H), 2.32 (s, 3H). ^{13}C NMR (150 MHz, DMSO-d_6) δ 186.42, 162.02 (d, J = 249.3 Hz), 150.55, 142.09, 137.25, 136.35, 134.00 (d, J = 8.4 Hz), 133.29, 130.37, 130.11 (dq, J = 30.0, J = 9 Hz), 129.66 (d, J = 4.7 Hz), 124.69, 123.11 (q, J = 271.5 Hz), 120.10 (d, J = 20.8 Hz), 115.17 (dd, J = 20.8, 4.7 Hz), 56.59, 55.73, 45.39. HRMS (ESI): *m/z* calcd. for $C_{20}H_{17}F_4N_2O$, [M + H]+, 377.1272; found: 377.1277.

2.3.19. (E)-3-((E)-4-fluoro-3-(trifluoromethyl)benzylidene)-1-methyl-5-(pyridin-4-ylmethylene)piperidin-4-one (5s)

Yellow powder; yield: 52 %; Mp:136.2 ~ 138.1 °C; ^{1}H NMR (600 MHz, DMSO-d_6) δ 8.66 (d, J = 6.1 Hz, 2H), 7.92 (d, J = 7.0 Hz, 1H),

7.90–7.82 (m, 1H), 7.67 (s, 1H), 7.65–7.57 (m, 1H), 7.53 (s, 1H), 7.45 (d, $J = 6.1$ Hz, 2H), 3.75 (s, 2H), 3.75 (s, 2H), 2.38 (s, 3H).^{13}C NMR (150 MHz, DMSO-d_6) δ 186.77, 159.28 (d, $J = 255.3$ Hz), 150.51, 142.14, 137.61, 137.18 (d, $J = 8.9$ Hz), 135.23, 133.10, 132.40, 132.15 (d, $J = 3.7$ Hz), 130.00 (q, $J = 4.6$ Hz), 124.66, 122.85(q, $J = 271.5$ Hz), 118.17 (dd, $J = 20.5$, 0.7 Hz), 117.48 (qd, $J = 31.5$, 12.0 Hz), 56.45, 56.30, 45.54. HRMS (ESI): *m/z* calcd. for $C_{20}H_{17}F_4N_2O$, [M + H]+, 377.1272; found: 377.1275.

2.4. Cell culture and CCK-8 assay for RAW 264.7cell cytotoxicity

Mouse RAW264.7 cells were kindly provided by Procell (Wuhan, China) and cultured in a complete medium consisting of DMEM supplemented with 10 % FBS and 1 % streptomycin/penicillin antibiotics. Cells of the logarithmic growth phase were recruited for the following tests. Detect cytotoxicity using the CCK-8 assay according to the manufacturer's instructions. Cells are grown and treated in 96-well plates and incubated with CCK-8 reagent for 1 h at 37 °C. Absorbance is measured at 450 nm.

2.5. Anti-inflammatory testing of all derivatives

RAW264.7 cells were randomly grouped. Cells were re-exposed for 24 h in the presence of 1.0 μg/mL LPS. After treatment, cells were collected and analyzed. TNF-α and IL-6 were assayed according to the ELISA double antibody sandwich kit assay instructions, and absorbance values at 450 nm were determined on the ELISA instrument after the assay. A standard curve was established for each measurement in pg/mL.

2.6. Western blotting

RAW264.7 cells (2.0×10^6 cells per well in 6-well plates) were exposed to the drug for 2.0 h and then to 1.0 μg/mL LPS for 24 h. Lysis was performed with a potent RIPA lysate containing a phosphatase inhibitor (RIPA lysate: phosphatase inhibitor = 99: 1). After complete sonication lysis on ice, centrifuge. After determining the protein concentration, the protein solution was boiled. Protein samples were added to a 10 % polyacrylamide gel for electrophoresis. The proteins were transferred onto PVDF membranes and incubated with 5 % skim milk for 2.0 h. Subsequently incubated with IκB-α, p-IκB-α, p65, p-p65, JNK2, p-JNK, p-38, p-p38, ERK, p-ERK, β-actin (antibodies purchased from Cell Signaling Technology, USA) antibodies at 4 °C overnight. Incubate with goat anti-rabbit IgG/HRP antibody (Solarbio, Beijing, China) for 1.0 h at room temperature. Testing was performed after using ECL developer (Novland Biopharma, Shanghai, China). Protein intensity was detected using Image Lab software and analyzed using ImageJ software.

2.7. Apoptosis assay

RAW264.7 cells were inoculated at a density of 2×10^5 cells/well in 12-well plates. The plates were then treated with **4 k** (0.275, 0.55, and 1.1 μM) for 24 h. Cells were collected in centrifuge tubes and washed twice with pre-cooled PBS. PBS was centrifuged and discarded. Cells were suspended in 200 mL of 1 binding buffer. 5 mL Annexin V-FITC and 5 mL of propidium iodide (BD Biosciences, San Jose, CA, USA) were then sequentially added to the solution. Apoptosis was rapidly detected by flow cytometry (BD FACS Cal ibur). Finally, cells were analyzed by flow cytometry.

2.8. Animals feeding

Male SPF Sprague-Dawley (SD) rats, 6 weeks old, 150–180 g, were purchased from Pengyue Experimental Animal Breeding Co Ltd [Qualification No. SYXK (Lu) 2018–0029, Jinan]. Animals were kept in animal houses at standard temperature (20 ± 1.0)°C, humidity (50 % ± 10 %) and 12 h photoperiod, given a standard diet, fed and watered ad libitum, and acclimatized for experiments 7 days before. All experimental-related operations were approved by the Experimental Animal Ethics Committee of Binzhou Medical University. All efforts were made to minimize the suffering of the animals used for the present experiments.

2.9. AIA induction and treatment

Rats were randomly separated into 6 different experimental groups with which 8 rats per group. Except for the control group, complete Freund's adjuvant (CFA) induced inflammation in rats by injecting 100 μL in the left hind paw after mixing in a vortex shake. To establish a model of adjuvant-induced rheumatoid arthritis (AIA), control rats were injected with an equal volume of saline at the same site. On day 10 after AIA induction, the control and AIA groups received intraperitoneal treatment Saline was used daily; the MTX group was treated orally. weekly with MTX (7.6 mg/kg suspended in 0.5 % CMC-Na) once a week; and the **4k** group was treated intraperitoneally.

2.10. Paw swelling and weight measurement

Body weight and paw swelling were measured in rats prior to modeling and every three days thereafter, and the arthritis index was evaluated. Paw swelling = post-inflammatory volume - pre-inflammatory volume. Grade 0: normal, no redness or swelling; Grade 1: redness or swelling of the toe joint; Grade 2: redness or swelling of the toe joint and metatarsal region; Grade 3: redness or swelling below the ankle joint; Grade 4: redness or swelling of the toe and ankle joints and joint dysfunction.

2.11. Arthritis index

On day 24, 2 h after the last dose, the rats were weighed and anesthetized (sodium pentobarbital; 50 mg/kg; i.p). The spleen and thymus of the rat were removed and euthanized. The spleen and thymus were weighed wet on an electronic balance in thousands to calculate the spleen and thymus factor. Immune organ index (%) = immune organ weight (mg) / rat body weight (g).

2.12. Immune index testing and blood processing

On day 24, 1 h after the last dose, the rats were given an intraperitoneal injection of 10 % chloral hydrate (1.15 mL/300 g) and blood was taken from the abdominal aorta after anesthesia, the blood samples were collected and left for two hours before centrifugation (3000 rpm, 4 °C, 10 min) and the supernatant was frozen at −80 °C. The spleen was taken and weighed wet on a one-thousandth of an electronic balance to calculate the spleen factor. Immune organ index (%) = immune organ weight (mg)/rat body weight (g).

2.13. Histopathological examination of joints

Rat ankle sections were entrusted to Rafael Biotechnology Co., Ltd. The left hind paw of rats was peeled, fixed in 4 % paraformaldehyde for 72 h, and decalcified by 12 % EDTA washing for 28 days. The samples were then routinely dehydrated, embedded, and cut into 4-μm paraffin sections, followed by HE staining and visualization by light microscopy. The degree of inflammatory cell infiltration was classified into four grades after pathological evaluation: grade 0: no inflammatory cell infiltration; grade 0: no inflammatory cell infiltration; grade; 1: weak inflammatory cell infiltration; grade; 2: mild infiltration; grade; 3: moderate inflammatory cell infiltration; and grade; 4: massive inflammatory cell infiltration. Synovial cell hyperplasia was classified into three grades, grade 0: normal without hyperplasia; grade 1: essentially normal with a small amount of hyperplasia; grade 2: moderate hyperplasia; and grade 3: significant synovial cell hyperplasia with massive

synovial cell attachment.

2.14. Statistics analysis

GraphPad Prism 8 software was used for plotting and bilateral t-tests, and ImageJ software was used to quantify protein expression. $^{\#\#}p < 0.01$, $^{\#\#\#}p < 0.001$ and $^{*}p < 0.05$, $^{**}p < 0.01$, $^{***}p < 0.001$ indicate statistically significant differences.

3. Results and discussion

3.1. Synthesis and structural characterization of target compounds

The synthetic strategy and structures of BAPs are shown in Scheme 1. One of the key raw materials is *N*-methyl-4-pperidone. According to the previous design, the aromatic aldehyde on one side is chosen as the raw material of 3-pyridine carboxaldehyde (**1a**) and 4-pyridine carboxaldehyde (**1b**), while the aromatic aldehyde on the other side was chosen to contain single fluorine, single trifluoromethyl or multiple substituents, such as 4-fluoro benzaldehyde (**2b**), 3-(trifluoromethyl) benzaldehyde (**2c**), 2,3-difluorobenzaldehyde (**2d**), 3,5-bis(trifluoromethyl)benzaldehyde (**2k**), 2-fluoro-3-(trifluoromethyl)benzaldehyde (**2l**), and so on. The titled compounds, **4a-s**, and **5a-s**, were synthesized under Claisen-Schmidt condensation catalyzed by dry HCl gas (Li et al., 2018a, 2018b). In the synthesis process, the ratio of the three raw materials was 1: 1: 1. Because of the formation of symmetric and asymmetric compounds, the target BAPs were purified by column chromatography, and the yield was only about 30 %. These yield rates are also similar to those reported in the literature. Then their chemical structures were confirmed by ^{1}H NMR, ^{13}C NMR and HRMS.

The spectral characteristics of the title compounds BAPs (**4a-s** and **5a-s**) share some common features because of their similar skeleton of (3*E*,5*E*)-3,5-bis(arylidene)-4-piperidone. In this study, BAP **4b** was taken as an example (Fig. 2). For the ^{1}H NMR spectra, the chemical shifts in 7.61 ppm and 7.62 ppm appear as two single peaks attributed to the two protons of the dissymmetrical α,β-unsaturated ketone pharmacophore on both sides of central piperidone. Meanwhile, due to the dissymmetry of BAP **4b**, ^{1}H NMR signals of two methylene groups of piperidone split into 3.75 ppm and 3.73 ppm. Similarly, in ^{13}C NMR spectra, the two methylene carbons split into two carbon signals, such as 56.74 ppm and 56.61 ppm. In addition, the characteristic peak with a chemical shift in 186.70 ppm should correspond to the carbonyl carbon atom of piperidone. BAP **4b** contains 4-fluorobenzene substitution, resulting in the presence of four split carbon signals in the carbon spectrum, at 162.87 ppm (d, $J = 246.1$ Hz), 133.75 ppm (d, $J = 2.0$ Hz), 133.38 ppm (d, $J = 8.6$ Hz), and 116.28 (d, $J = 21.3$ Hz). In conclusion, the above NMR signals prove the structural correctness of BAP **4b**. These results further confirm the correctness of their structures.

3.2. Screening for cytotoxic and anti-inflammatory activity

In this study, the CCK-8 assay was used as a preliminary cytotoxicity assessment in vitro. All experiments were repeated three times in parallel and the mean value of survival was taken. The survival rates of RAW264.7 cells treated with the title compounds (1.1 μM) are shown in Fig. 3. After treatment with 1.1 μM of BAPs, the survival rate of RAW264.7 cells was more than 85 %, which proved the newly synthesized BAPs were not significantly toxic to RAW264.7 cells. Only compounds 4b, **4e**, **5k**, and **5n** were more toxic to RAW264.7 cells, resulting in only 85–90 % cell survival, but this does not affect the screening for the next anti-inflammatory activity.

In RA, TNF-α and IL-6 are the main pro-inflammatory cytokines that trigger bone damage. TNF-α and IL-6 can cause bone damage by binding to receptors and indirectly inducing the expression of RANKL (Marahleh et al., 2019; Labib et al., 2020). Therefore, blocking TNF-α or IL-6 delays or halts the progression of bone destruction in RA. The inflammation

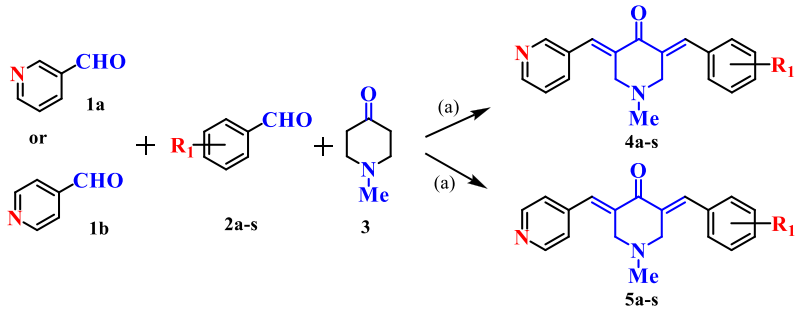

Compounds	R1	Compounds	R1
2a, 4a, 5a	3-F	**2k, 4k, 5k**	3-CF_3, 5-CF_3
2b, 4b, 5b	4-F	**2l, 4l, 5l**	2-F, 3-CF_3
2c, 4c, 5c	3-CF_3	**2m, 4m, 5m**	2-F, 4-CF_3
2d, 4d, 5d	2-F, 3-F	**2n, 4n, 5n**	2-F, 5-CF_3
2e, 4e, 5e	3-F, 4-F	**2o, 4o, 5o**	2-F, 6-CF_3
2f, 4f, 5f	2-F, 4-F	**2p, 4p, 5p**	3-F, 4-CF_3
2g, 4g, 5g	2-F, 5-F	**2q, 4q, 5q**	3-F, 5-CF_3
2h, 4h, 5h	2-F, 6-F	**2r, 4r, 5r**	4-F, 2-CF_3
2i, 4i, 5i	3-F, 5-F	**2s, 4s, 5s**	4-F, 3-CF_3
2j, 4j, 5j	2-CF_3, 4-CF_3	-	-

Scheme 1. Synthetic route of compounds **4a-s** and **5a-s**. Reagents and conditions: (a) 20 % NaOH/MeOH, T: 25 °C, 3–5 h.

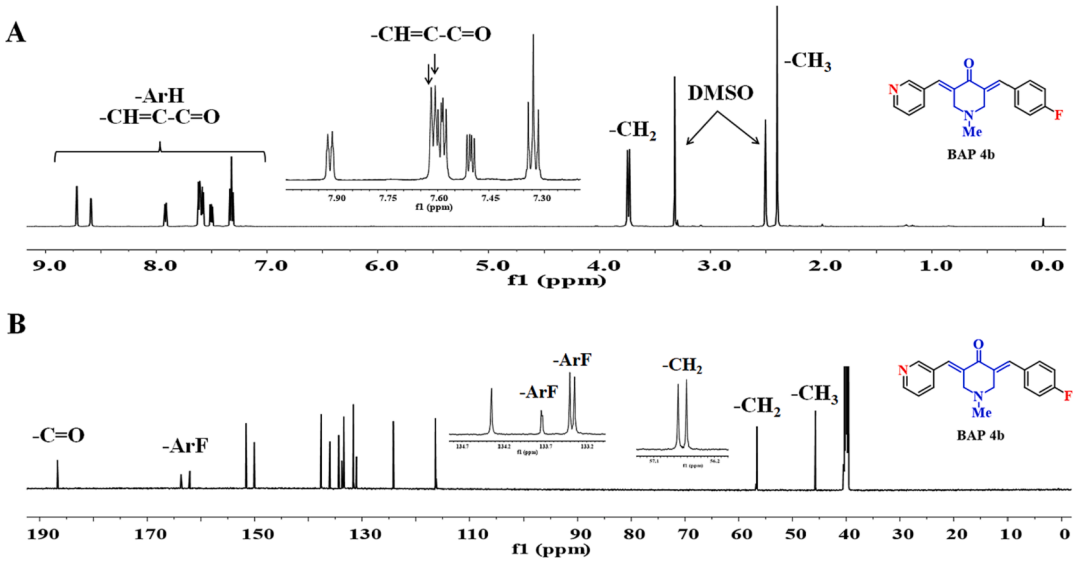

Fig. 2. (A) ^{1}HNMR spectrum and proton attribution of **4b**; (B) ^{13}CNMR spectrum and carbon attribution of **4b**.

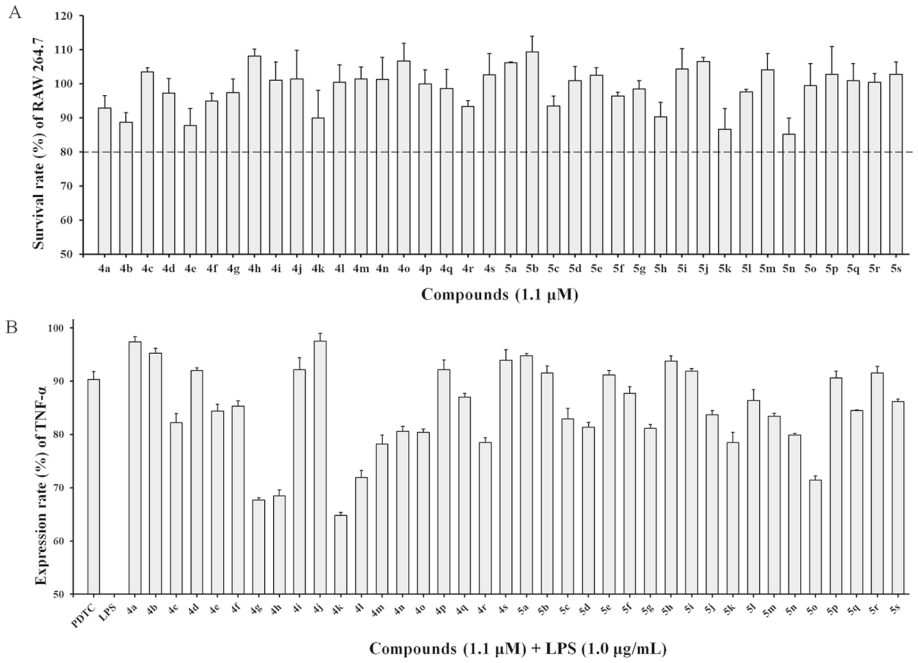

Fig. 3. (A) Survival rate (%) of RAW 264.7 cells treated with target compounds (5.0 μM). (B) Expression rate (%) of the inflammatory cytokine TNF-α in LPS-stimulated RAW264.7 macrophages with target compounds (5.0 μM) and LPS (1 μg/mL) by ELISA analysis. PDTC (5.0 μg/mL) was used as a positive control.

model established by LPS-stimulated RAW 264.7 cell is used in basic research of anti-inflammatory drugs, which can help to screen drug targets and anti-inflammatory active ingredients and contribute to the development of anti-inflammatory drugs. PDTC (Pyrrolidine dithiocarbamate, μM) was used as a positive control. All experiments were performed three parallel times and the mean expression rates (%) are shown in Fig. 3. We see that the TNF-α expression rate in LPS-stimulated RAW 264.7 cell after PDTC (5.0 μM) exposure was 90.3 ± 1.5 %.

For the monofluorinated substituted BAPs **4a**, **4b**, **5a**, and **5b**, they had little to no inhibitory effect on the release of TNF-α, which expression rates were all higher than the positive control PDTC. For bis-fluorinated substituted **4d-i** and **5d-i**, 2,5-F-3-pyridyl-substituted **4g** and 2,6-F-3-pyridyl-substituted **4h** exhibited better anti-inflammatory activity, and the TNF-α expression rate in LPS-stimulated RAW 264.7 cell after treatment with **4g** and **4h** were only 67.7 % and 68.5 %, respectively. More interestingly, the 4-pyridyl-substituted **5g** also exhibited an expression rate of 81.2 %.

After changing the substituent to 3-CF_3-substituted BAP **4c** and **4d,** this inhibitory effect was significantly improved, leading to a release of TNF-α of 82.2 % and 82.9 %, respectively. There is no difference in inhibitory effect whether 3-pyridyl or 4-pyridyl substituted in BAPs. For 2,4-CF_3-substituted **4j** and **5j,** the inhibitory effect barely improves. When replacing the substituent position with 3,5-CF_3, BAPs **4k** and **5k** were obtained. Surprisingly, they showed a significant improvement in anti-inflammatory activity, whose TNF-α expression rate in LPS-stimulated RAW 264.7 cells can reach 64.8 % and 78.5 %, respectively. Especially for **4k**, exhibited the strongest inhibitory effect against TNF-α expression in all title BAPs. This indicates that 3-pyridine substitution is more favorable than 4-pyridine substitution in anti-inflammatory activity. In general, the results indicated that the

substituent effect of BAPs has a significant influence on TNF-α expression in LPS-stimulated RAW 264.7 cells.

To further examine the substituent effect of BAPs, we selected a batch of aromatic aldehydes containing -F and -CF_3 groups as raw materials to obtain a series of fluorine- and trifluoromethyl-substituted BAPs, **4l–s**, and **5l–s**. Screening for anti-inflammatory activity showed 2-F-3-CF_3-substituted **4l**, 2-F-4-CF_3-substituted **4m**, 2-F-5-CF_3-substituted **5n**, 2-F-6-CF_3-substituted **5o**, and 4-F-2-CF_3-substituted **4r** exhibited moderate inhibitory effect against TNF-α expression. Their expression rate in LPS-stimulated RAW 264.7 cells was 71.9 %, 78.2 %, 79.9 %, 71.4 %, and 78.5 %, respectively. Compared to that of **4k**, there is no significant improvement.

Based on the above results, the preliminary structure–activity relationship (SAR) of anti-inflammatory activities could be summarized. Firstly, mono-fluoro-substituted BAPs are less active than monotrifluoromethyl-substituted BAPs. Secondly, the 3,5-CF_3 substituent significantly outperformed other substituents. Thirdly, 3-pyridine substituents significantly outperformed 4-pyridine substituents. Combining toxicity and anti-inflammatory activity, **4k** (Fig. 4A) was selected to continue the next biological evaluation.

The anti-IL-6 effect is shown in Fig. 4, where IL-6 expression decreased to 72 % after PDTC (5 μM) exposure. Using BAP **32** (1.1 μM), a lead compound with good anti-inflammatory activity, as a control, the expression rate decreased to 65 % after exposure, which was lower than PDTC. BAP **4k** expression rate decreased to 59 % after exposure, which was better than PDTC with BAP **32**. The present results show that **4k** can effectively reduce the concentration of TNF-α and IL-6 and have a good anti-inflammatory effect.

3.3. 4k induce RAW264.7 cells apoptosis in a dose-dependent manner

To further corroborate the effect of **4k** on apoptosis, the results of **4k** on RAW264.7 cells were analyzed by flow cytometry using the Membrane Associated Protein V/PI assay kit. Double staining for membrane-linked protein V and PI allows differentiation between live cells (membrane-linked protein V-/PI-), early apoptotic cells (annexin V+/PI-

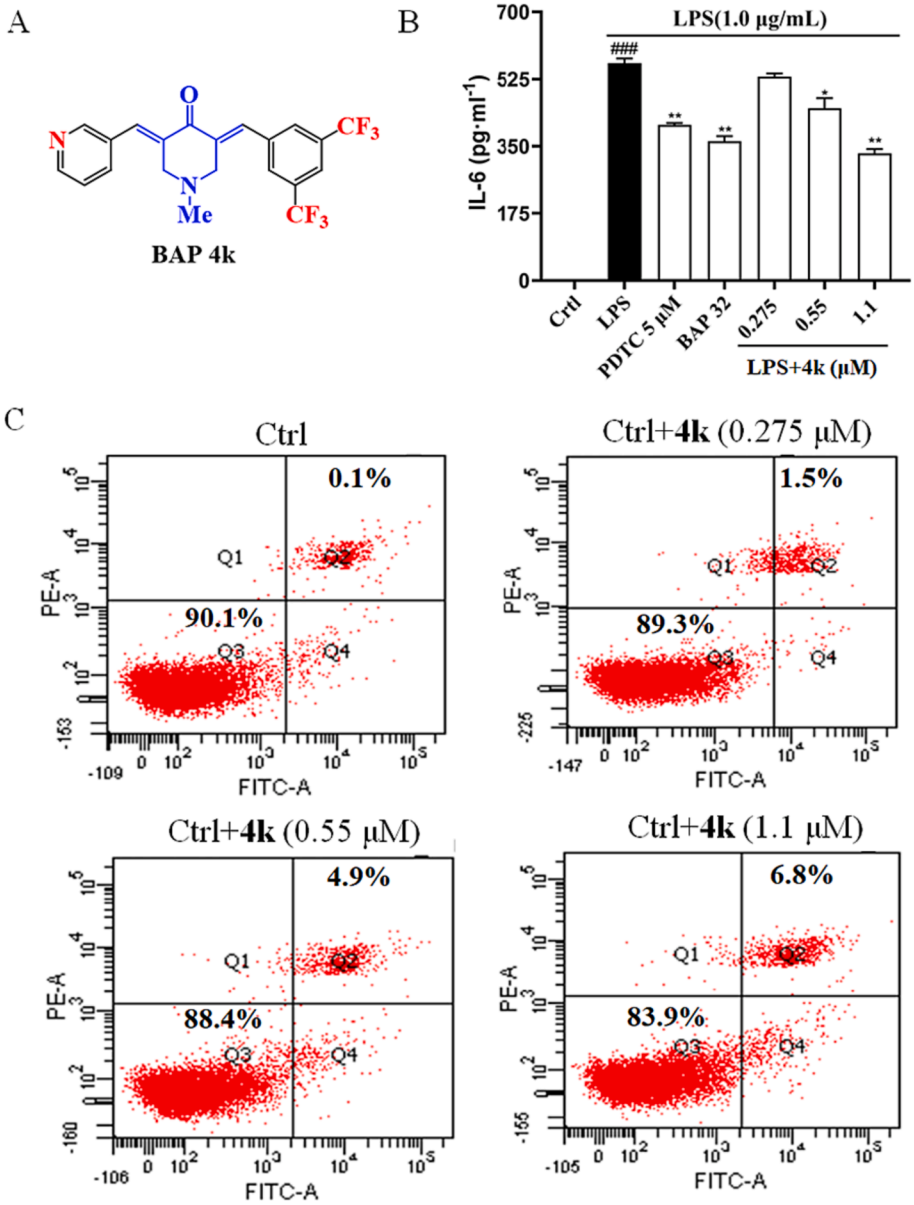

Fig. 4. (A) The structure of BAP **4k**. (B) The expression levels of IL-6 in LPS-induced RAW 264.7 cells through ELISA analysis. PDTC and BAP **32** were used as positive controls. Statistical significance relative to the LPS group is indicated: *: $P < 0.1$; **: $P < 0.01$. Compared with Ctrl group: ###: $P < 0.001$. (C) RAW 264.7 cells were incubated with **4k** and analyzed for apoptosis by flow cytometry.

), late apoptotic cells (annexin V+/PI +), and necrotic cells (membrane linked protein V-/PI +). As shown in Fig. 4C, there was almost no apoptosis of Ctrl cells, while apoptosis only was 1.5 %, 4.9 %, and 6.8 %, after treatment with different doses of **4k** (0.275, 0.55, 1.1 μM, respectively). Apoptosis increased with increasing dose. The present results further corroborate that **4k** (1.1 μM) was not significantly toxic to RAW264.7 cells.

3.4. 4k impacts paw swelling, arthritic index values, and body weight in AIA rats

NF-κB and MAPK signaling pathways are both classical inflammatory pathways, which can promote the proliferation and differentiation of osteoclasts, thus causing bone erosion and bone destruction (Jiang et al., 2019; Behl et al., 2022). Therefore, NF-κB and MAPK signaling pathways play an important role in the disease development of RA, which are important targets for the treatment of RA and other chronic immune-mediated inflammatory diseases. Normally, inactivated NF-κB is inactivated in the cytoplasm, while inflammatory stimuli (LPS or other external stimuli) lead to the release and nuclear translocation of NF-κB and phosphorylation of the p65-IκBα complex (Zhang et al., 2018; Liu et al., 2020; Zhou et al., 2022; Yu et al., 2020). MAPK signaling pathway is closely related to NF-κB. So, we endeavored to reveal whether the inhibitory effect of compound **4k** on inflammation is related to the activation of NF-κB and MAPK. Therefore, we further detected the expression of NF-κB-related and MAPK-related proteins, including IκB-α, p65, JNK, ERK, and p38. Analysis of IκB-α, p65 in LPS-treated RAW264.7 cells by protein blotting revealed (Fig. 5) that 24 h LPS intervention induced IκB-α, p65 protein phosphorylation and upregulated JNK, ERK, p38 protein phosphorylation compared to control. After different concentrations (0.275, 0.55, and 1.1 μM) of **4k**, the LPS-induced protein phosphorylation expression levels decreased significantly as expected. As shown in Fig. 5A, compared with the LPS-induced group, the expression levels of NF-κB-related IκB-α and p65 proteins were significantly decreased and exhibited a clearly dose-dependent (Fig. 5B and 5C). As shown in Fig. 5D, the expression levels of MAPK-related JNK, ERK, and p38 proteins were significantly decreased sequentially with increasing concentrations of **4k**. A clearly dose-dependent can be found (Fig. 5E-G). The result indicated that **4k** significantly inhibited the LPS-induced phosphorylation of NF-κB-related IκB-α, p65 proteins, and MAPK-related JNK, ERK, and p38 proteins. This also indicates that **4k** may inhibit LPS-induced NF-κB and MAPK activation with a dose-dependent in RAW264.7 cells.

3.5. 4k impacts paw swelling, arthritic index values, and body weight in AIA rats

The development of RA is characterized by joint erythema, pain, and synovial hyperplasia. The adjuvant-based arthritis model is a classic model of RA in which rats develop swelling and pain, synovial hyperplasia, and bone damage after inflammation is induced by using a complete Freund's adjuvant (Choudhary et al., 2018; Li et al., 2021). Compound **4k** showed favorable results in the assay of the LPS-induced anti-inflammatory activity of RAW264.7. To further determine the anti-RA efficacy of **4k**, this study was conducted to establish an adjuvant-type arthritis model using complete Fever's adjuvant as an inducer for efficacy studies (Fig. 6A). In this study, the CFA was established with a significant increase in paw swelling and arthritis index (Logashina et al.,

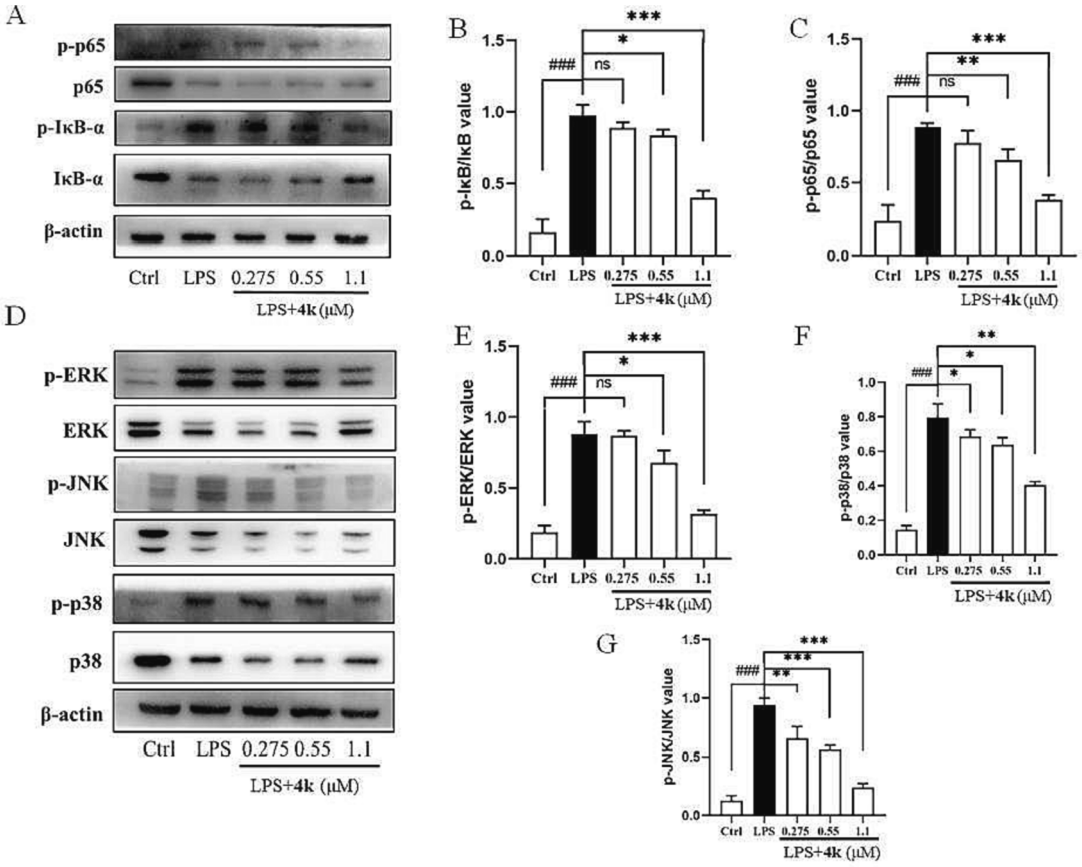

Fig. 5. (A) The expression of NF-κB-related IκBα and p65 phosphorylation in LPS-induced RAW264.7 cells by **4k**; (B-C) Relative expression of p-IκBα and IκBα, p-p65 and p65; (D) The expression of MAPK-related JNK, ERK, p38 proteins and their phosphorylation in LPS-induced RAW264.7 cells by **4k**; (E-G) Relative expression of p-ERK and ERK, p-JNK and JNK, p-p38 and p38; Compared with LPS alone group: *: $P < 0.05$; **: $P < 0.01$; ***: $P < 0.001$. Compared with Ctrl group: ###: $P < 0.001$.

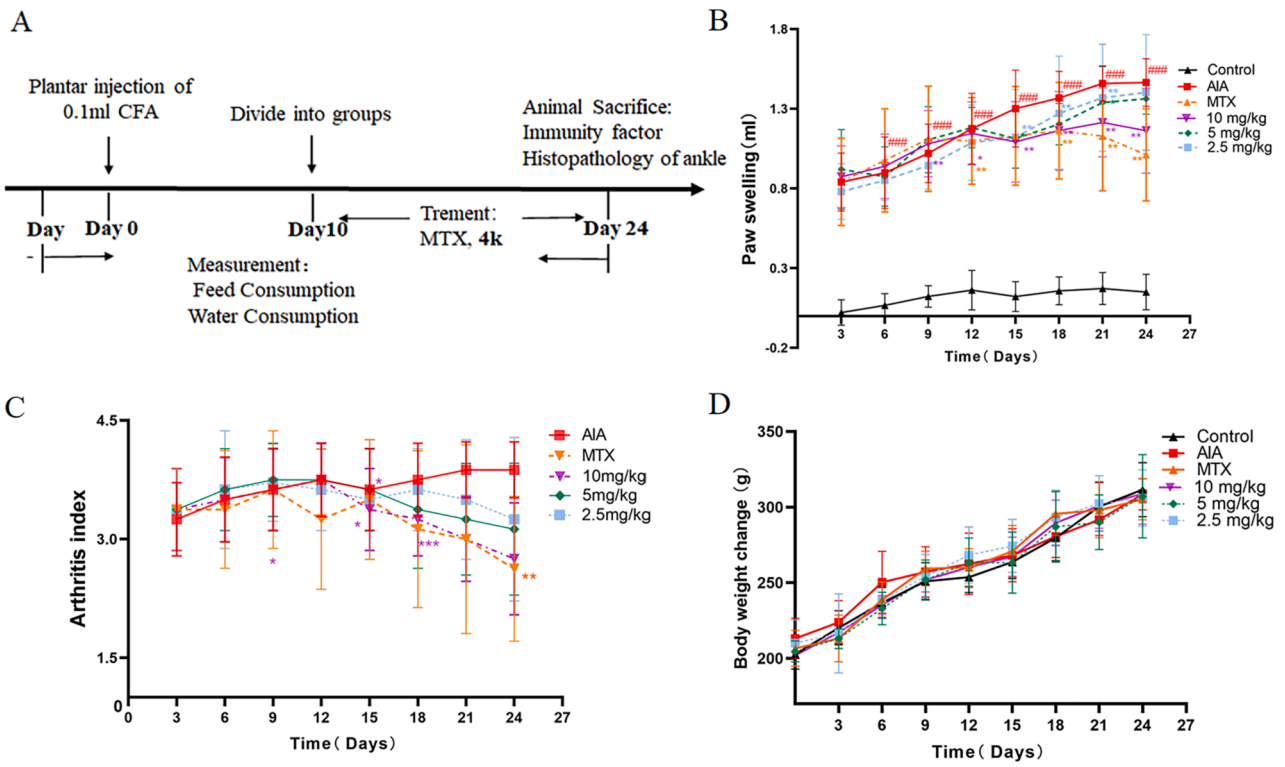

Fig. 6. (A) Experimental process of the adjuvant-based arthritis model. (B-D) Degree of paw swelling, arthritis index, and body weight changes in rats. B: Paw swelling; C: Arthritis index; D: Body weight change; Data are represented as mean ± SEM, n = 5. ##p < 0.01, ###p < 0.001 compare with control group.

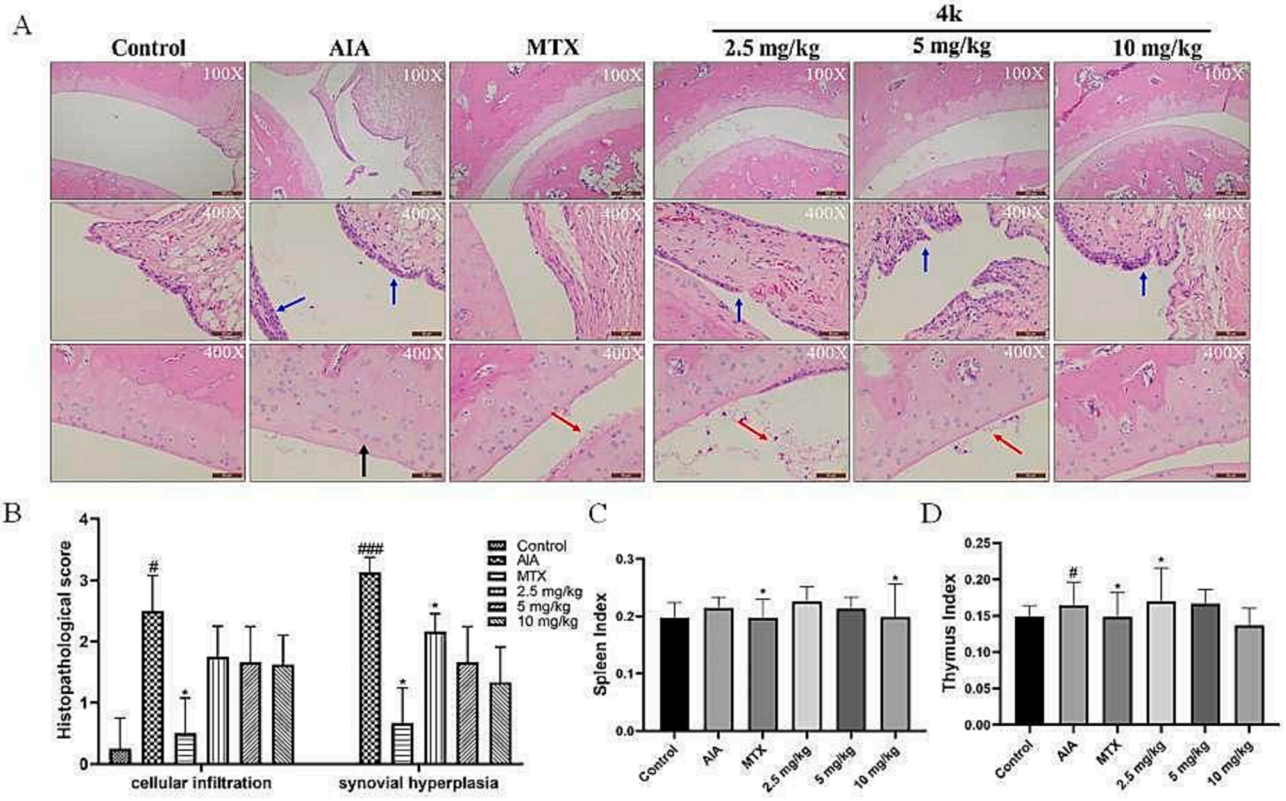

Fig. 7. Effect of **4k** on the histopathology of rat joints. (A) Haematoxylin and eosin-stained sections of joint tissues; (B) inflammatory scores of joint tissues. (C, D) The impact of **4k** on immune organ Spleen (C) and thymus (D) index values in AIA Model Rats. Data are represented as mean ± SD, n = 3. ##p < 0.01, ###p < 0.001 compared with control group, *p < 0.1, **p < 0.01, ***p < 0.001 compared with AIA group.

2021). Therefore, paw swelling and arthritis indices are important indicators of inflammation measurements. Firstly, paw volumes of all rats were measured every 3 days, starting from day 0 (Fig. 6B). The methotrexate (MTX) and **4k** (10 mg/kg) groups inhibited foot swelling in rats from 15 days compared with the AIA. However, by 24 days, the **4k** group (10 mg/kg) paw swelling was significantly lower than that of the AIA group. Secondly, to assess the development of inflammation, we performed a simultaneous assessment of the arthritis coefficient. There was no significant difference in the arthritis scores of the AIA group when the scores were started after administration (Fig. 6C) on day 12. With continuous administration, MTX with **4k** (10 mg/kg) showed a significant advantage in the inhibition of paw swelling. Finally, body weight is an important indicator of in vivo experimental toxicity of the compounds assessed, with body weight changes able to give an important indication of toxicity to the rats. Body weight measurements were performed every three days starting from day 10 (Fig. 6D). Compared with the AIA and control groups, the MTX group showed a significant decrease in body weight, which may be related to the toxicity of MTX, but there was no significant effect on body weight after injection of **4k**.

3.6. 4k alters AIA-associated histopathological changes in rat joints

During the development of CFA, ankle synovial hyperplasia and inflammatory cell infiltration are important indicators for evaluating the condition. Therefore, we decided to observe the ankle joint of rats by HE staining. First, Fig. 7A shows no exudate in the joint cavity of the control group and no inflammatory cell infiltration in the connective tissue of the joint capsule. The surface was covered with a single or double layer of synovial cells without hyperplasia. Unlike the control group, the AIA group had a large amount of inflammatory cell infiltration and cellular degeneration in the joint capsule connective tissue (black arrows), and the surface was covered with synovial cell hyperplasia (blue arrows). The MTX group has an insignificant inflammatory cell infiltrate with mild surface synovial cell hyperplasia with inflammatory exudate (red arrow). The **4k** group has synovial hyperplasia with a small amount of inflammatory cell infiltration. Secondly, histopathology showed that inflammatory cell infiltration and synovial cell proliferation were significantly reduced in the **4k** group in a dose-dependent manner (Fig. 7B). The results indicated that **4k** effectively inhibited synovial proliferation and inflammatory cell infiltration in rat ankle joints and suppressed CFA inflammation.

3.7. The impact of 4k on immune organ index values in AIA model rats

Significantly increased splenic index values in AIA relative to control, animals at the end of the experimental period are consistent with the immunological basis of the disease (Zeng et al., 2023). Relative to AIA model animals, MTX-treated rats exhibited a significant decrease in immune organ index values consistent with impaired immune function in treated animals. The dose of **4k** (10 mg/kg) slightly reduced thymic index values (Fig. 7D), but did not affect splenic index values (Fig. 7C).

4. Conclusions

Rheumatoid arthritis (RA) is a peripheral immune disease, whereas the usual clinical drugs are limited to NSAIDs and immunosuppressive drugs. Inhibition of inflammation-related NF-κB and MAPK activation could treat RA to some extent. The natural product curcumin and its analogs have been extensively studied for their anti-inflammatory and anti-cancer activity, including anti-RA effects. Recently, mang 3,5-bis (aryl)-4-piperidone derivatives (BAPs) were obtained by design modification of curcumin in our group, and some fluorine- and pyridyl-substituted BAPs exhibited promising potential anti-inflammatory activity. In this paper, thirty-eight dissymmetric fluorine and pyridyl-substituted BAPs were synthesized and evaluated as potential anti-inflammatory agents for the treatment of RA by inhibition of MAPK and NF-κB signaling pathways in this study. It is hoped that our study will yield potentially versatile agents for the treatment of inflammatory diseases such as RA.

A preliminary structure–activity relationship was summarized and discovered 3,5-CF_3 and 3-pyridyl-substituted **4k** exhibited less toxicity and more potential anti-inflammatory activity. We also found that anti-rheumatoid effects were related to the inhibition of NF-κB and MAPK signaling pathways. Mechanistic studies show that lead compound **4k** effectively inhibited LPS-induced NF-κB and MAPK activation by suppressing LPS-induced phosphorylation levels of p65, IκBα, JNK, ERK, and p38 in RAW264.7 cells. Based on the rat AIA model, **4k** significantly inhibited the growth of paw swelling and arthritis index in rats. More importantly, **4k** did not affect body weight and splenic index values, which indicates that it had a better therapeutic effect and no significant toxicity in CFA rats. Histopathologically, **4k** effectively inhibited synovial hyperplasia and inflammatory cell infiltration in rat ankle joints and suppress the development of CFA rats. Overall, this study demonstrated that curcumin analog, BAP **4k**, had relatively potential anti-RA effects. It may be developed as a potential multifunctional agent for the clinical treatment of inflammatory diseases such as RA.

Funding

We are grateful for financial support from Shandong Provincial Natural Science Foundation (Nos. ZR2022MH159, ZR2023MH022, ZR2023MH190), College Youth Innovation Science and Technology Support Programme of Shandong province (No. 2020KJK003). This study was financially supported by Key Laboratory of Medical Antibacterial Materials of Shandong Province.

Declaration of competing interest

The authors declare that they have no known competing financial interests or personal relationships that could have appeared to influence the work reported in this paper.

References

Al-Warhi, T., Al-Karmalawy, A.A., Elmaaty, A.A., Alshubramy, M.A., Abdel-Motaal, M., Majrashi, T.A., Asem, M., Nabil, A., Eldehna, W.M., Sharaky, M., 2023. Biological evaluation, docking studies, and in silico ADME prediction of some pyrimidine and pyridine derivatives as potential $EGFR^{WT}$ and $EGFR^{T790M}$ inhibitors. J. Enzyme Inhib. Med. Chem. 38 (1), 176–191. https://doi.org/10.1080/14756366.2022.2135512.

Behl, T., Upadhyay, T., Singh, S., Chigurupati, S., Alsubayiel, A.M., Mani, V., Vargas-De-La-Cruz, C., Uivarosan, D., Bustea, C., Sava, C., Stoicescu, M., Radu, A.F., Bungau, S. G., 2021. Polyphenols targeting MAPK mediated oxidative stress and inflammation in rheumatoid arthritis. Molecules 26 (21), 6570. https://doi.org/10.3390/molecules26216570.

Behl, T., Rana, T., Alotaibi, G.H., Shamsuzzaman, M., Naqvi, M., Sehgal, A., Singh, S., Sharma, N., Almoshari, Y., Abdellatif, A.A.H., Iqbal, M.S., Bhatia, S., Al-Harrasi, A., Bungau, S., 2022. Polyphenols inhibiting MAPK signalling pathway mediated oxidative stress and inflammation in depression. Biomed. Pharmacother. 146, 112545 https://doi.org/10.1016/j.biopha.2021.112545.

Bottini, N., Firestein, G.S., 2013. Duality of fibroblast-like synoviocytes in RA: passive responders and imprinted aggressors. J. Nat. Med. 9 (1), 24–33. https://doi.org/10.1038/nrrheum.2012.190.

Chen, G., Mao, Y., Wang, J., Zhou, J., Diao, L., Wang, S., Zhao, W., Zhu, X., Yu, X., Zhao, F., Liu, X., Liu, M., 2023. Phillyrin ameliorated collagen-induced arthritis through inhibition of NF-κB and MAPKs pathways in fibroblast-like synoviocytes. Arab. J. Chem. 16, 104844 https://doi.org/10.1016/j.arabjc.2023.104844.

Choudhary, N., Bhatt, L.K., Prabhavalkar, K.S., 2018. Experimental animal models for rheumatoid arthritis. Immunopharmacol. Immunotoxicol. 40, 193–200. https://doi.org/10.1080/08923973.2018.1434793.

Cong, W., Sun, Y., Sun, Y.F., Yan, W.B., Zhang, Y.L., Gao, Z.F., Wang, C.H., Hou, G.G., Zhang, J.J., 2021. Trifluoromethyl-substituted 3,5-bis(arylidene)-4-piperidones as potential anti-hepatoma and anti-inflammation agents by inhibiting NF-κB activation. J. Enzyme Inhib. Med. Chem. 36 (1), 1622–1631. https://doi.org/10.1080/14756366.2021.1953996.

Gao, C.L., Hou, G.G., Liu, J., Ru, T., Xu, Y.Z., Zhao, S.Y., Ye, H., Zhang, L.Y., Chen, K.X., Guo, Y.W., Pang, T., Li, X.W., 2020. Synthesis and target identification of benzoxepane derivatives as potential anti-neuroinflammatory agents for ischemic stroke. Angew. Chem. Int. Ed. Engl. 59 (6), 2429–2439. https://doi.org/10.1002/anie.201912489.

He, Y., Li, W., Hu, G., Sun, H., Kong, Q., 2018. Bioactivities of EF24, a novel curcumin analog: a review. Front. Oncol. 8, 614. https://doi.org/10.3389/fonc.2018.00614.

Labib, M.B., Fayez, A.M., El-Nahass, E.S., Awadallah, M., Halim, P.A., 2020. Novel tetrazole-based selective COX-2 inhibitors: design, synthesis, anti-inflammatory activity, evaluation of PGE_2, TNF-α, IL-6 and histopathological study. Bioorg. Chem. 104, 104308 https://doi.org/10.1016/j.bioorg.2020.104308.

Li, L., Pan, Z., Ning, D., Fu, Y., 2021. Rosmanol and carnosol synergistically alleviate rheumatoid arthritis through inhibiting TLR4/NF-κB/MAPK pathway. Molecules 27, 78. https://doi.org/10.3390/molecules27010078.

Li, N., Xin, W.Y., Yao, B.R., Cong, W., Wang, C.H., Hou, G.G., 2018a. *N*-phenylsulfonyl-3,5-bis(arylidene)-4-piperidone derivatives as activation NF-κB inhibitors in hepatic carcinoma cell lines. Eur. J. Med. Chem. 155, 531–544. https://doi.org/10.1016/j.ejmech.2018.06.027.

Li, N., Xin, W.Y., Yao, B.R., Wang, C.H., Cong, W., Zhao, F., Li, H.J., Hou, Y., Meng, Q.G., Hou, G.G., 2018b. Novel dissymmetric 3,5-bis(arylidene)-4-piperidones as potential antitumor agents with biological evaluation in vitro and in vivo. Eur. J. Med. Chem. 147, 21–33. https://doi.org/10.1016/j.ejmech.2018.01.088.

Littlejohn, E.A., Monrad, S.U., 2018. Early diagnosis and treatment of rheumatoid arthritis. Prim. Care 45 (2), 237–255. https://doi.org/10.1016/j.pop.2018.02.010.

Liu, W., Hou, C., Li, J., Ma, X., Zhang, Y., Hu, M., Huang, Y., 2020. Discovery of talmapimod analogues as polypharmacological anti-inflammatory agents. J. Enzyme Inhib. Med. Chem. 35, 187–198. https://doi.org/10.1080/14756366.2019.1693703.

Logashina, Y.A., Palikova, Y.A., Palikov, V.A., Kazakov, V.A., Smolskaya, S.V., Dyachenko, I.A., Tarasova, N.V., Andreev, Y.A., 2021. Anti-Inflammatory and analgesic effects of TRPV1 polypeptide modulator APHC3 in models of osteo- and rheumatoid arthritis. Mar. Drugs 19, 39. https://doi.org/10.3390/md19010039.

Marahleh, A., Kitaura, H., Ohori, F., Kishikawa, A., Ogawa, S., Shen, W.R., Qi, J., Noguchi, T., Nara, Y., Mizoguchi, I., 2019. TNF-α directly enhances osteocyte RANKL expression and promotes osteoclast formation. Front. Immunol. 10, 2925. https://doi.org/10.3389/fimmu.2019.02925.

Meanwell, N.A., 2018. Fluorine and fluorinated motifs in the design and application of bioisosteres for drug design. J. Med. Chem. 61 (14), 5822–5880. https://doi.org/10.1021/acs.jmedchem.7b01788.

Nugroho, A.E., Morita, H., 2014. Circular dichroism calculation for natural products. J. Nat. Med. 68, 1–10. https://doi.org/10.1007/s11418-013-0768-x.

Pourhabibi-Zarandi, F., Shojaei-Zarghani, S., Rafraf, M., 2021. Curcumin and rheumatoid arthritis: A systematic review of literature. Int. J. Clin. Pract. 75 (10), e14280.

Sun, Y., Gao, Z.F., Wang, C.H., Hou, G.G., 2019. Synthesis, crystal structures and anti-inflammatory activity of fluorine-substituted 1,4,5,6-tetrahydrobenzo[*h*]quinazolin-2-amine derivatives. Acta Crystallogr. C Struct. Chem. 75 (Pt 8), 1157–1165. https://doi.org/10.1107/S2053229619010118.

Sun, Y., Zhou, Y.Q., Liu, Y.K., Zhang, H.Q., Hou, G.G., Meng, Q.G., Hou, Y., 2020. Potential anti-neuroinflammatory NF-κB inhibitors based on 3,4-dihydronaphthalen-1(2*H*)-one derivatives. J. Enzyme Inhib. Med. Chem. 35 (1), 1631–1640. https://doi.org/10.1080/14756366.2020.1804899.

Swallow, S., 2015. Fluorine in medicinal chemistry. Prog. Med. Chem. 54, 65–133. https://doi.org/10.1016/bs.pmch.2014.11.001.

Wang, Q., Ye, C., Sun, S., Li, R., Shi, X., Wang, S., Zeng, X., Kuang, N., Liu, Y., Shi, Q., Liu, R., 2019. Curcumin attenuates collagen-induced rat arthritis via anti-inflammatory and apoptotic effects. Int. Immunopharmacol. 72, 292–300. https://doi.org/10.1016/j.intimp.2019.04.027.

Wei, X., Zhou, R., Chen, Y., Ma, G., Yang, Y., Lu, C., Xu, W., Hu, W., 2022. Systemic pharmacological verification of Baixianfeng decoction regulating TNF-PI3K-Akt-NF-κB pathway in treating rheumatoid arthritis. Bioorg. Chem. 119, 105519 https://doi.org/10.1016/j.bioorg.2021.105519.

Yao, B.R., Sun, Y., Chen, S.L., Suo, H.D., Zhang, Y.L., Wei, H., Wang, C.H., Zhao, F., Cong, W., Xin, W.Y., Hou, G.G., 2019. Dissymmetric pyridyl-substituted 3,5-bis(arylidene)-4-piperidones as anti-hepatoma agents by inhibiting NF-κB pathway activation. Eur. J. Med. Chem. 167, 187–199. https://doi.org/10.1016/j.ejmech.2019.02.020.

Yu, H., Lin, L., Zhang, Z., Zhang, H., Hu, H., 2020. Targeting NF-κB pathway for the therapy of diseases: mechanism and clinical study. Signal Transduct. Target. Ther. 5, 209. https://doi.org/10.1038/s41392-020-00312-6.

Zeng, W., Shen, C., Mo, S., Ni, C., Lin, Y., Fang, Y., Yang, H., Luo, G., Xiao, L., Zhan, R., Yan, P., 2023. The Effective Treatment of Purpurin on Inflammation and Adjuvant-Induced Arthritis. Molecules 28, 366. https://doi.org/10.3390/molecules28010366.

Zhang, L., Shi, L., Soars, S.M., Kamps, J., Yin, H., 2018. Discovery of novel small-molecule inhibitors of NF-κB signaling with antiinflammatory and anticancer properties. J. Med. Chem. 61 (14), 5881. https://doi.org/10.1021/acs.jmedchem.7b01557.

Zhou, Y., Wang, S., Luo, H., Xu, F., Liang, J., Ma, C., Ren, L., Wang, H., Hou, Y., 2022. Aflatoxin B1 induces microglia cells apoptosis mediated by oxidative stress through NF-κB signaling pathway in mice spinal cords. Environ. Toxicol. Pharmacol. 90, 103794 https://doi.org/10.1016/j.etap.2021.103794.

Zhu, H., Xu, T., Qiu, C., Wu, B., Zhang, Y., Chen, L., Xia, Q., Li, C., Zhou, B., Liu, Z., Liang, G., 2016. Synthesis and optimization of novel allylated mono-carbonyl analogs of curcumin (MACs) act as potent anti-inflammatory agents against LPS-induced acute lung injury (ALI) in rats. Eur. J. Med. Chem. 121, 181–193. https://doi.org/10.1016/j.ejmech.2016.05.041.